



## Review

## Cathode materials of metal-ion batteries for low-temperature applications

Xiaowan Pang<sup>a,\*</sup>, Baigang An<sup>a,\*</sup>, Shumin Zheng<sup>b,\*</sup>, Bao Wang<sup>b,\*</sup><sup>a</sup> School of Chemical Engineering, University of Science and Technology Liaoning, 185 Qianshanzhong Road, Anshan 114051, China<sup>b</sup> State Key Laboratory of Biochemical Engineering, Institute of Process Engineering, Chinese Academy of Sciences, Beijing 100190, China

## ARTICLE INFO

## Article history:

Received 10 February 2022

Received in revised form 7 April 2022

Accepted 21 April 2022

Available online 26 April 2022

## Keywords:

Lithium-ion battery

Multivalent metal-ion battery

High-energy cathode material

Ultralow temperature

Electrochemical performance

## ABSTRACT

Energy storage devices have been developed greatly in recent years. Developing forward, they are expected to operate stably in electric vehicles, electric grids, military equipment, and aerospaces in various climates. Unfortunately, these areas require batteries to be repeatedly and periodically exposed to sub-zero temperatures, even extremely low temperatures ( $-40\text{ }^{\circ}\text{C}$  or lower). The low temperature reduces the kinetics of all the activation processes of the batteries, leading to increased impedance and polarization, and loss of battery energy and power, thus restricting their performance. Developing new cathode materials is one of the main strategies to alleviate the low-temperature restrictions. A conventional lithium-ion battery is the most attractive system, which is more adaptive to the practical low-temperature application now. Sodium-ion batteries, magnesium-ion batteries, and zinc-ion batteries, which have the advantages of low cost and high safety, are considered potential substitutes for lithium-ion batteries, the electrochemical performance of these batteries at low-temperature has been conducted extensively. This review provides an overview of lithium-ion batteries, sodium-ion batteries, magnesium-ion batteries, and zinc-ion batteries that can work normally in low-temperature environments, with emphasis on various high-energy cathode materials, mainly including polyanionic compounds, layered oxides, spinel oxides, Prussian blue, and Prussian blue analogs. Specifically, we propose how the conventional low-temperature charge-transfer resistance can be overcome. However, these chemistries also present their own unique challenges at low temperatures. This article discusses the advantages and disadvantages of these materials, as well as the main challenges and strategies for applying them to batteries at low temperatures so that the batteries can still discharge efficiently.

© 2022 Elsevier B.V. All rights reserved.

## Contents

1. Introduction	2
2. Cathode material for lithium-ion battery	3
2.1. Polyanion cathode	3
2.2. Oxide cathode	4
3. Cathode materials for sodium batteries	6
3.1. Prussian blue and Prussian blue analogs cathode	6
3.2. Polyanion cathode	8
3.3. Oxide cathode	10
4. Cathode material for magnesium-ion battery	11
4.1. Polyanion cathode	12
4.2. Oxide cathode	13
5. Cathode materials for zinc-ion batteries	14
5.1. Oxide cathode	14

\* Corresponding authors.

E-mail addresses: [bgan@ustl.edu.cn](mailto:bgan@ustl.edu.cn) (B. An), [smzheng@ipe.ac.cn](mailto:smzheng@ipe.ac.cn) (S. Zheng), [baowang@ipe.ac.cn](mailto:baowang@ipe.ac.cn) (B. Wang).

5.2. Other materials .....	16
6. Conclusions and outlook .....	17
Declaration of Competing Interest .....	18
Acknowledgments .....	18
References .....	18

## 1. Introduction

The contradiction between world energy supply and demand has become increasingly prominent. In energy consumption, fossil energy accounts for a large part. Although fossil energy, such as oil and coal can still meet human needs in this century, nevertheless, it is important to keep in mind that resources will eventually be exhausted [1,2]. Therefore, there is an urgent need to research, develop and apply clean and environmentally friendly new energy sources, such as solar energy, hydropower, and tidal energy, to reduce pollution and improve energy efficiency. The development of electrical energy storage (EES) systems is the key to integrating intermittent renewable energy into continuous controllable power transmission [3]. With the development of science and technology, people's demand and desire for reliable EES systems are increasing. However, sub-zero low-temperature is the critical obstacle for the wide application of EES systems. Some major areas, such as electric vehicles, smart grids, and space exploration [4,5], requires EES systems to be repeatedly and periodically exposed to sub-zero temperatures, even an extremely low temperature of  $-80\text{ }^{\circ}\text{C}$ , as shown in Fig. 1 [6]. Thus, EES systems are expected to work normally in a cold climate.

As one of the most important energy storage devices, lithium-ion batteries (LIBs) are widely used in portable electronic applications and other fields. When the lithium-ion battery works at a low temperature, the kinetic speed of chemical and electrochemical reactions decreases significantly. As the temperature decreases, the charge transfer is hindered, resulting in low conductivity that affects the battery performance and rate discharge performance [7], such as a significant decrease in the discharge plateau and a significant decrease in the discharge capacity [8,9]. When the temperature dropped further to minus  $20\text{ }^{\circ}\text{C}$ , the battery even stopped working [10]. Therefore, the use of commercial Li-ion batteries at  $-20\text{ }^{\circ}\text{C}$  is rarely recommended [11]. When the temperature drops to  $-30\text{ }^{\circ}\text{C}$ , the discharge capacity of the battery is 87.0% of the discharge capacity at room temperature, and its stored energy is only about 70% of the ordinary environment. When used in a low temperature environment for a long time, or in an ultra-low temperature environment of  $-40\text{ }^{\circ}\text{C}$ , the battery will be "frozen" and cause permanent damage [12]. Applications such as military, deep-sea diving, and aerospace must ensure that lithium-ion batteries perform well over an extremely wide temperature range. For example, while the operating temperature of military-grade batteries is between  $-50\text{ }^{\circ}\text{C}$  and  $60\text{ }^{\circ}\text{C}$ , such lithium-ion batteries have not been fully optimized and developed, and the energy, power, and cycle life are significantly reduced in low temperature environments. The use of lithium-ion batteries is severely restricted in some cold regions [13–18].

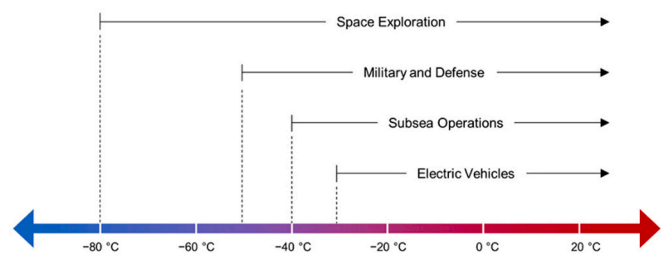


Fig. 1. Application-specific low-temperature conditions within which battery systems must be capable of operating.

Among other types of metal-ion batteries, sodium is characterized by abundant resources and wide geographical distribution [19], and sodium-ion batteries are comparable to lithium-ion batteries in large-scale electrical energy storage. Meanwhile, multivalent metal-ion batteries such as  $\text{Mg}^{2+}$  and  $\text{Zn}^{2+}$  have emerged as promising candidates for large-scale replacement of Li-ion batteries [20]. Compared with lithium, the content of magnesium in the crust is about 2 wt% [21], which is more abundant than lithium. Because metallic magnesium does not allow dendritic circulation, it is easily recovered when it is used as an anode [22]. Zinc metal is very stable and abundant and can be directly used as the anode. However, the above metal-ion batteries also have their own problems at low temperatures. For example, sodium-ion batteries suffer from slow  $\text{Na}^+$  diffusion kinetics at low temperatures [23], a large capacity decay [24], and a significant decrease in energy and power density [25]. At low temperature, magnesium ion batteries have problems with slow ion transport, easy structure collapse, difficult insertion and extraction of magnesium ions, and insufficient electrochemical performance [26]. Zinc-ion batteries suffer from slow ion migration, reduced charge transfer kinetics, and capacity fading at low temperatures [27] due to the high freezing point of the water-based electrolyte, low ionic conductivity, and poor interfacial freezing of the water-based electrolyte and electrodes [28].

In order to alleviate the problems of low-temperature batteries, lithium-ion batteries mostly use internal or external heating strategies to increase the battery temperature to ensure that it can operate at a relatively favorable and stable temperature [29]. However, although this thermal management system can make the battery work normally at a lower temperature to a certain extent, the external heating efficiency is low, the power consumption is too large, and the temperature gradient is easily generated inside the battery, which affects the service life of the lithium-ion battery [30]. The heating control mechanism is complex and there are potential safety hazards [31,32]. In novel battery design and battery chemistry, by improving bulk and interfacial properties, for example, introducing low-melting co-solvents into electrolytes to improve conductivity at low temperatures [33–37]; fluorination to weaken the solvation effect of ion-solvent complexation [38]; optimization of interface and membrane additives to control resistance, etc [39]. At the same time, the electrodes have been modified, such as nanoization to shorten ion diffusion paths or surface treatments with conducting polymers to improve conductivity [40–42].

The related reports on the improvement of Na-ion, Mg-ion, and Zn-ion batteries at low temperature are far less abundant than those of Li-ion batteries. In low-temperature sodium-ion batteries, the nanostructure of the cathode material can be designed, and the ultrafine nano-size effect can be used to greatly increase the battery capacity and achieve excellent low-temperature performance [43]; modification and doping of electrode materials can reduce  $\text{Na}^+$  migration energy barrier and promote  $\text{Na}^+$  migration [44,45]; use  $\text{Na}^+$  solvent co-intercalation strategy to accelerate  $\text{Na}^+$  diffusion kinetics and reduce activation energy [46]; in addition, unique porous structures can also be constructed to encapsulate nanoparticles, facilitate ion and electron transfer, etc. [47]. Magnesium-ion batteries can improve their low-temperature performance by expanding the interchain distance and increasing ion diffusivity [48]; using  $\text{Mg}^{2+}$  as a charge carrier, organic electrode materials were designed to store ions [49]; solvents with low viscosity and low melting point were chosen to resist the freezing of electrolyte solutions [143]. For low-

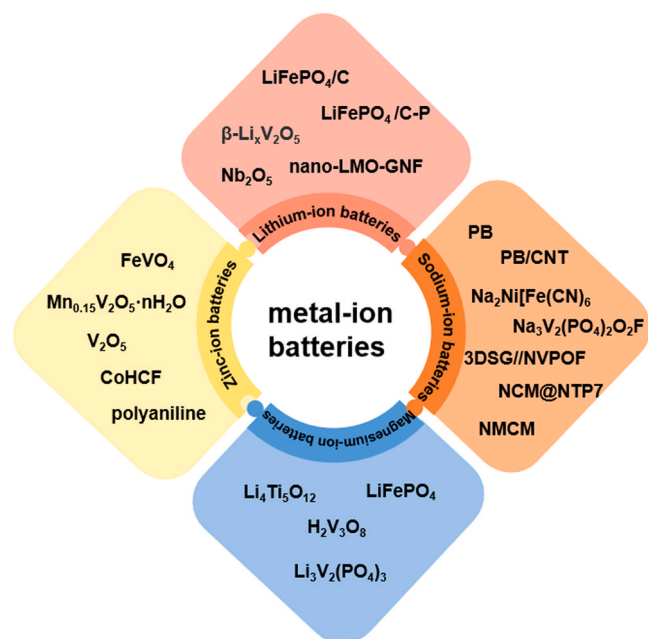


Fig. 2. Cathode materials for metal-ion batteries are normally used at low temperatures.

temperature zinc-ion batteries, the freezing point of the electrolyte can be lowered by adding deep eutectic solvents [50]; developing mixed hydrogel electrolytes to suppress their freezing and low ionic conductivity [51]; the use of intercalation materials can promote  $\text{Zn}^{2+}$  intercalation, improve kinetics and structural stability, etc. [52].

In recent years, the performance of metal-ion batteries at low temperatures can be improved through continuous improvements in low-temperature battery design [53]. According to the current works, these candidate batteries can maintain stable capacity and good cycle performance at low temperatures by improving and optimizing cathode materials [54,55]. In Fig. 2, among the cathode materials, Prussian blue (PB, PB=CNT, etc.), polyanionic compounds ( $\text{LiFePO}_4$ ,  $\text{Li}_3\text{V}_2(\text{PO}_4)_3$ (LVP),  $\text{Na}_3\text{V}_2(\text{PO}_4)_2\text{O}_2\text{F}$ , etc.) and oxides ( $\text{Mn}_{0.15}\text{V}_2\text{O}_5 \cdot n\text{H}_2\text{O}$ ,  $\text{V}_2\text{O}_5$ ,  $\text{FeVO}_4$ , etc.) have been widely studied and applied to low-temperature batteries to achieve high performance. In this regard, I will focus on the challenges that these cathode materials need to face when they are applied to batteries at low temperatures, the corresponding strategies, and discuss their electrochemical properties such as specific capacity, cycle stability, and capacity retention under low-temperature conditions.

## 2. Cathode material for lithium-ion battery

At present, the development of high-performance energy storage systems for portable electronic devices, vehicles, and smart grids is the most pressing challenge. Lithium-ion batteries have become the most successful system to meet energy storage needs due to their well-developed technology. In recent years, the cathode materials used in low-temperature lithium-ion batteries mainly include polyanion cathode materials and oxide cathodes. However, polyanionic cathode materials have low capacity and poor electrical conductivity [63], and oxide cathode materials have poor cycle stability and low ionic conductivity [88]. These disadvantages prevent Li-ion batteries from guaranteeing good electrochemical performance at low temperatures.

### 2.1. Polyanion cathode

Polyanionic compounds are usually composed of  $(\text{XO}_4)^{n-}$  or its derivatives  $(\text{X}_m\text{O}_{3m+1})^{n-}$  ( $\text{X} = \text{S}, \text{P}, \text{Si}, \text{As}, \text{Mo}$  or  $\text{W}$ ) and  $\text{MeO}_x$  ( $\text{Me}$  is a

transition metal) polyhedra. Its cathode materials have the advantages of tunable voltage and long-term cycling stability but suffer from the problems of moderate capacity and low conductivity [56,57]. Most of the research on the operation of lithium-ion battery cathodes at low temperatures is based on the polyanion cathode material lithium iron phosphate  $\text{LiFePO}_4$  electrodes.  $\text{LiFePO}_4$  is considered as the main material for Li-ion batteries for electrical transport because of its sufficient specific capacity, excellent cycling performance, thermal stability, and low self-discharge [58–60]. Theoretically,  $\text{LiFePO}_4$  exchanges with the electrolyte on all surfaces, but the actual Li-ions can only move toward the crystal along the [010] direction, which seriously affects the diffusivity of Li ions [61,62]. At the same time,  $\text{LiFePO}_4$  has poor electrical conductivity [63], and as the activity of the material decreases, these shortcomings are amplified and cause a sharp drop in capacity, this seriously hinders the development and application of  $\text{LiFePO}_4$  [64–66], especially its low-temperature electrochemical performance. To overcome these drawbacks, it is generally accepted to coat  $\text{LiFePO}_4$  particles with conductive coatings (usual carbon) [67,68] or metal oxides with high conductivity [69,70], as well as to minimize the size of  $\text{LiFePO}_4$  particles [71,72].

Coating conductive coatings on the  $\text{LiFePO}_4$  surface is an effective method to improve the low temperature capacity of cathode materials. On the one hand, it is to build an electron transport network to improve the conductivity of the cathode material [73,74], and on the other hand, it is to stabilize the structure of the material by reducing the polarization during charging and discharging. Carbon coating is a relatively mature method to improve the electrochemical performance of  $\text{LiFePO}_4$ . First, the porous form of carbon after high temperature pyrolysis facilitates the penetration of the electrolyte and can effectively inhibit the oxidation of  $\text{Fe}^{2+}$ , improving the purity of the phase [75,76]. Secondly, the conductive network constructed by carbon coating can effectively improve the conductivity of  $\text{LiFePO}_4$ . Last but not least, the carbon coating can not only improve the degree of graphitization but also build a better conductive network through complementary advantages, thereby optimizing the low temperature performance of  $\text{LiFePO}_4$ . In addition, studies have shown that surface modification by providing conductive additives is beneficial to improving the limitations of low-temperature electrochemical performance due to extremely low intrinsic conductivity [77,78]. The conductive additive can not only improve the conductivity but also act as a protective layer to prevent the electrolyte from directly contacting  $\text{LiFePO}_4/\text{C}$ , thereby reducing the charge transfer resistance and improving the structural stability.

Cai et al. [79] chose titanium silicon carbide ( $\text{Ti}_3\text{SiC}_2$ ) as a conductive additive and formed a composite material by coating thin carbon with  $\text{LiFePO}_4$ (LFP) particles and  $\text{Ti}_3\text{SiC}_2$ (TSC) particles by a suspension mixing method. This modification is a very effective way to repair the conductive network. By connecting the active particles and the conductive layer, the active material can be protected from erosion by the electrolyte. When the  $\text{Ti}_3\text{SiC}_2$  content is 4%, the  $\text{Ti}_3\text{SiC}_2$ -modified  $\text{LiFePO}_4/\text{C}$  sample has the lowest charge transfer resistance and the highest diffusion coefficient. At this time, the electrical conductivity of the nanocomposite is only  $3.4\mu\text{S}\text{cm}^{-1}$ , but its low-temperature performance is better, and it also has excellent rate performance and good cycle stability. At a temperature of  $-20^\circ\text{C}$  and a discharge rate of 1 C, the initial capacity is  $98.4\text{mAhg}^{-1}$ . After 100 cycles, the capacity retention rate is close to 97%. Therefore, TSC modification is an effective way to improve the low-temperature performance of LFP/C.

Cui et al. [80] used graphite and triphenylphosphine to promote the formation of a carbon network structure, and successfully prepared a  $\text{LiFePO}_4/\text{C-P}$ (LFP/C-P) composite cathode through a simple sol-gel method, and discussed the carbon-containing coating and phosphorus-doped LFP/C-P composite material at low temperature electrochemical performance [81]. To compare the performance of

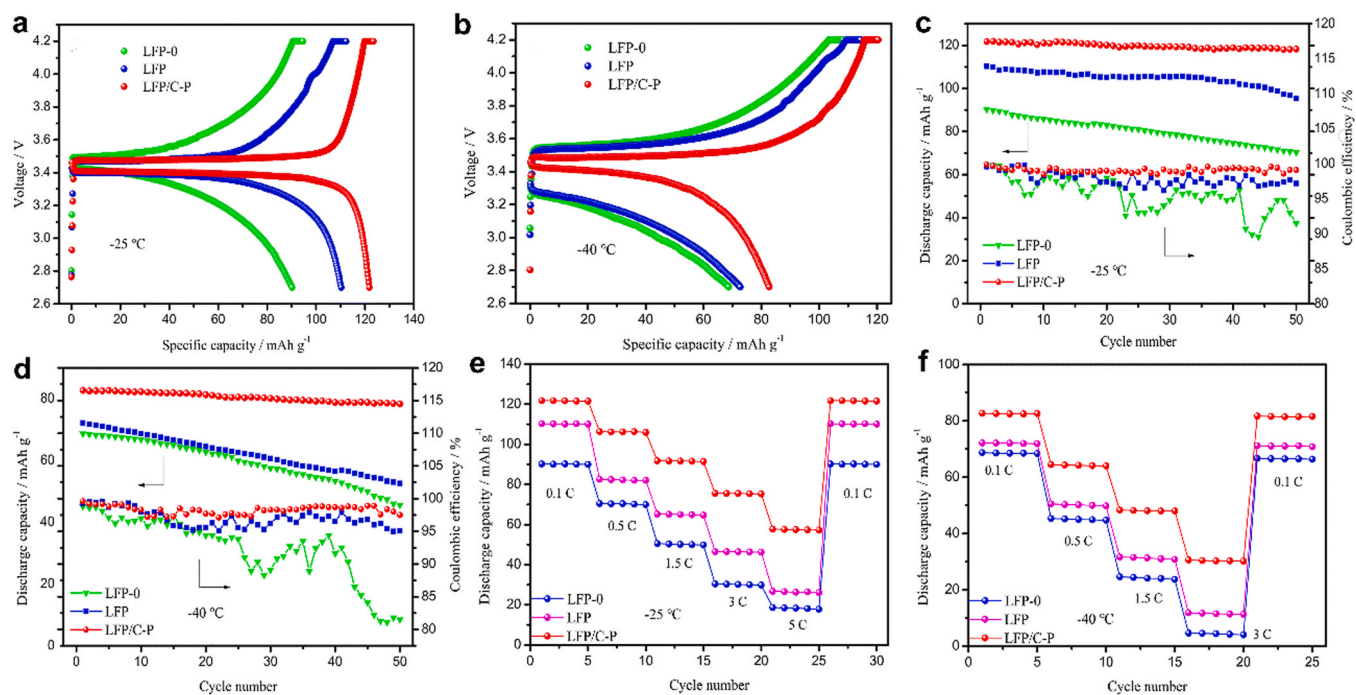


**Fig. 3.** First charge-discharge curves of LFP-0, LFP, and LFP/C-P composites at 0.1 C by charging at room temperature and discharging at  $-25\text{ }^{\circ}\text{C}$  a and  $-40\text{ }^{\circ}\text{C}$  b, respectively. Cycle performance curves of LFP-0, LFP, and LFP/C-P composites at 0.1 C  $-25\text{ }^{\circ}\text{C}$  c, and  $-40\text{ }^{\circ}\text{C}$  d. Rate capability curves of LFP-0, LFP, and LFP/C-P composites at rates of  $-25\text{ }^{\circ}\text{C}$  e and  $-40\text{ }^{\circ}\text{C}$  f.

synthetic materials, commercial LFP and synthetic LFP are used as a comparison. Fig. 3a-b shows the initial charge and discharge curves of the three materials at a low temperature when the current density is 0.1 C. Through comparison, it can be seen that the discharge capacity and coulombic efficiency of LFP/C-P composites are both maximum at low temperatures. The discharge capacity at  $-25\text{ }^{\circ}\text{C}$  is  $121.8\text{mAhg}^{-1}$ , the coulombic efficiency is 99.5%, the discharge capacity at  $-40\text{ }^{\circ}\text{C}$  is  $82.7\text{mAhg}^{-1}$  and the coulombic efficiency is 73.3%. This shows that the phosphorus-doped carbon coating can improve the discharge capacity and coulombic efficiency of LFP materials at low temperatures. In Fig. 3c-d, it can be observed that the capacity decay rate of LFP-0 and LFP is faster than that of the LFP/C-P electrode at  $-25\text{ }^{\circ}\text{C}$  and  $-40\text{ }^{\circ}\text{C}$ , exhibiting excellent coulomb efficiency and higher discharge capacity. To further study the rate performance of these three materials, Fig. 3e-f shows the rate performance at different temperatures. All LFP/C-P materials have higher discharge capacities. This is because the phosphorus-doped carbon coating establishes interconnected channels and forms an effective conductive network, thereby increasing the ion diffusion rate and discharge capacity. In addition, this result indicates that the addition of appropriate phosphorus and carbon can help improve the low-temperature rate performance. Yao et al. [82] prepared a novel  $\text{LiFePO}_4/\text{C}$  composite using in-situ graphitized carbon cages to encapsulate nano-sized  $\text{LiFePO}_4$  spheres, exhibiting excellent electronic conductivity and excellent capacity. It has excellent rate capability at room temperature and excellent capacity retention even at  $-40\text{ }^{\circ}\text{C}$ .

Reducing the particle size is helpful to improve the low temperature capacity of  $\text{LiFePO}_4$ . The particle size reduction can shorten the diffusion paths of  $\text{Li}^+$  and electrons, facilitate the intercalation/extraction process of Li, and accelerate the electron transfer rate to a certain extent [83,84]. At the same time, the large specific surface area of the small particles can fully contact the electrolyte and promote the rapid diffusion of  $\text{Li}^+$  between the solid and liquid phases [85]. Zhao et al. [86] systematically studied the effect of particle size of  $\text{LiFePO}_4/\text{C}$  material on its low temperature performance. The results show that the capacity increases from  $52.4\text{mAhg}^{-1}$  to  $105.6\text{mAhg}^{-1}$  when the

particle size decreases from  $1.63\text{ }\mu\text{m}$  to  $1.45\text{ }\mu\text{m}$  at 0.2 C at  $-20\text{ }^{\circ}\text{C}$ . This reflects that particle size reduction can improve low temperature performance. However, smaller particle size generates more side reactions and also requires a large amount of binder, which inevitably leads to lower energy [87].

## 2.2. Oxide cathode

Oxide cathodes have a high capacity, but usually exhibit disadvantages such as poor cycle stability and low ionic conductivity [88]. In the past few decades, research on vanadium oxide and its derivatives as electrodes has attracted great interest. Vanadium pentoxide ( $\text{V}_2\text{O}_5$ ) and intercalated vanadium oxide bronzes ( $\text{M}_x\text{V}_2\text{O}_5$ , M¼alkali, alkaline-earth, or transition metal cations) have received extensive attention and research due to their unique structural flexibility, safety, and high specific capacity [89]. It is generally believed that in the  $\text{Li}_x\text{V}_2\text{O}_5$  system, the intercalation of lithium-ions into two-dimensional layered  $\text{V}_2\text{O}_5$  will cause changes in its internal structure, phase transitions, and a substantial decrease in capacity [90], which makes it unable to maintain good performance at low temperatures. In contrast,  $\beta\text{-Li}_x\text{V}_2\text{O}_5$  has a monoclinic tunnel structure with a unique rigid three-dimensional frame [91], shows good structural reversibility, and has been proven to have potential as a lithium battery cathode [92].

Wang et al. [93] prepared a three-dimensional tunnel-type  $\beta\text{-Li}_x\text{V}_2\text{O}_5$  cathode material for lithium-ion batteries. Compared with layered  $\text{V}_2\text{O}_5$ , this cathode material provides more reversible Li insertion sites. The electrochemical performance of the  $\beta\text{-Li}_x\text{V}_2\text{O}_5$  cathode from  $-40\text{ }^{\circ}\text{C}$  to  $-25\text{ }^{\circ}\text{C}$  was investigated by the constant current charge-discharge test in Fig. 4a. The results show that the electrode has a discharge capacity of  $147.2\text{mAhg}^{-1}$  and  $123.8\text{mAhg}^{-1}$  at  $-20\text{ }^{\circ}\text{C}$  and  $-40\text{ }^{\circ}\text{C}$ , respectively. Compared with other types of cathodes,  $\beta\text{-Li}_x\text{V}_2\text{O}_5$  has a relatively high capacity at low temperature. Fig. 4b shows that the battery maintains high capacity after 100 cycles at low temperature: the capacity retention is 88.6% at  $-40\text{ }^{\circ}\text{C}$  and 79.5% at  $-20\text{ }^{\circ}\text{C}$ . One of the main factors contributing to its unusual low-

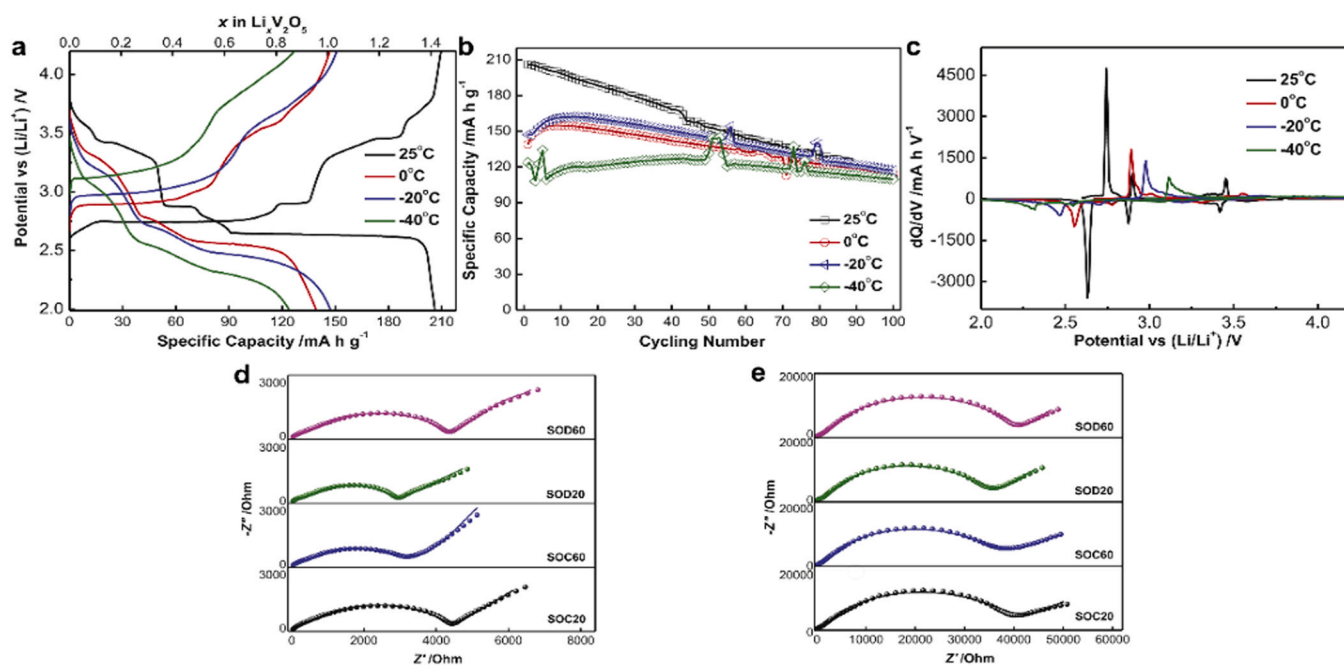


**Fig. 4.** a The 1st discharge/charge curves of  $\beta$ - $\text{Li}_x\text{V}_2\text{O}_5$  electrodes at different temperatures under 0.1 C; b Cycling performance of  $\beta$ - $\text{Li}_x\text{V}_2\text{O}_5$  electrodes at different temperatures under 0.1 C; c  $dQ/dV$  curves of  $\beta$ - $\text{Li}_x\text{V}_2\text{O}_5$  electrodes at 1st cycle under 0.1 C; d Nyquist plots of  $\beta$ - $\text{Li}_x\text{V}_2\text{O}_5$  electrode at different states of charge/discharge under different temperatures: d -20 °C; e -40 °C.

temperature cycling stability lies in its unique three-dimensional tunnel structure, which provides a large number of reversible lithium intercalation/extraction sites. However, when the battery is at an extremely low temperature, electrochemical polarization can lead to difficulties in Li insertion/extraction, which in turn brings irreversible structural changes to the 3D tunneling structure. It can be observed in Fig. 4c that with the decrease of temperature, the peak and area of redox peaks gradually decrease, the specific capacity decreases, and the potential separation of oxidation peak and reduction peak increases, which reflects the slow electrochemical kinetics at low temperature. The electrochemical impedances of  $\beta$ - $\text{Li}_x\text{V}_2\text{O}_5$  at different temperatures are depicted in Fig. 4d-f. The results showed that the charge transfer resistance gradually increased and the electrochemical reaction kinetics decreased gradually with the decrease in temperature. Therefore, the main factors limiting the low-temperature performance of  $\beta$ - $\text{Li}_x\text{V}_2\text{O}_5$  lie in the slow charge transfer kinetics and the solid-state Li diffusion in  $\text{Li}_x\text{V}_2\text{O}_5$  particles. In order to make  $\beta$ - $\text{Li}_x\text{V}_2\text{O}_5$  have better electrochemical performance at low temperature, measures such as surface modification, particle size minimization, or incorporation of conductive materials can be taken.

Although intercalation compounds are commonly used electrodes in lithium-ion batteries, there is a problem with slow interfacial reactions at low temperatures. The intercalation pseudocapacitor materials combine the redox reaction of the battery and fast kinetics that are not limited by semi-infinite diffusion. Therefore, their diffusion in bulk materials is faster than in traditional intercalation compounds, and there is no phase change [94,95]. This intercalation behavior may help to avoid the challenge of slow  $\text{Li}^+$  desolvation and diffusion from the electrolyte to the body electrode and can be used as a substitute for traditional intercalation compounds at low temperatures [96]. The study found that the  $\text{Li}^+$  intercalation pseudocapacitance mechanism was found in  $\text{Nb}_2\text{O}_5$ . The pseudocapacitance reaction of this mechanism is accompanied by the intercalation reaction to achieve rapid insertion kinetics. Therefore, the  $\text{Nb}_2\text{O}_5$  material has a very high low-temperature charge storage performance. Dong et al. [97] used nanosized  $\text{Nb}_2\text{O}_5$  as the cathode of a rechargeable battery that can be operated at a

low temperature of -75 °C. Benefiting from the surface-controlled charge storage process, the inherently embedded pseudocapacitance behavior of  $\text{Nb}_2\text{O}_5$  can be maintained even at low temperatures. Fig. 5a shows the charge/discharge curve at -75 °C under different current densities. At 0.05 C, the battery has a high capacity of  $121\text{mAhg}^{-1}$  at 0.5 C, and its capacity retention rate is approximately 50%. In Fig. 5b, after cycling 100 times at -75 °C with a current density of 0.5 C, the coulombic efficiency can reach 100%, and it has excellent cycle stability. Fig. 5c-d shows that the battery can still provide a high power density of  $1178\text{Wkg}^{-1}$  at a low temperature of -75 °C, and its power retention rate can be as high as 90.7% at 0.05 C.

Transition metal oxide manganese-based materials with spinel structure, especially lithium manganate ( $\text{LiMn}_2\text{O}_4$ ), have the advantages of good stability, high power, non-toxicity, and low cost. However, the Jahn-Teller effect can lead to a phase transition of  $\text{LiMn}_2\text{O}_4$  (cubic system-tetragonal system), and a large volume change occurs during cycling, thereby reducing the capacity of  $\text{LiMn}_2\text{O}_4$  [98]. During the discharge process,  $\text{Mn}^{2+}$  undergoes a disproportionation reaction, and the generated  $\text{Mn}^{2+}$  and  $\text{Mn}^{4+}$  are easily soluble in the electrolyte, resulting in the reduction of the positive active material and the capacity decay. Li-ion batteries have been hindered by their limited charge-discharge rate, stability, temperature range, and safety. To overcome these problems, nanostructured electrodes have received extensive attention. It has a large contact area and a short diffusion path [99], which can improve the charge-discharge capacity and kinetics [100,101], but there are still some disadvantages. For example, due to the increase of the interfacial area and the occurrence of side reactions, the cycle life is reduced; the volume energy density is low, etc. Therefore, an efficient strategy is needed to preserve the nanoparticle structure of cathode materials while promoting efficient electronic and ionic conducting network structures. Chen et al. [102] utilized ethyl cellulose to stabilize dispersions of nano-LMO particles and graphene nanoflakes (GNFs) to realize nano-LMO/graphene composite (n-LG) cathodes. By coating graphene on the nano-LMO surface, a thin and stable SEI layer can be formed, which can inhibit the occurrence of side reactions and avoid the dissolution of Mn. This dense network structure enhances charge transfer and exhibits excellent rate

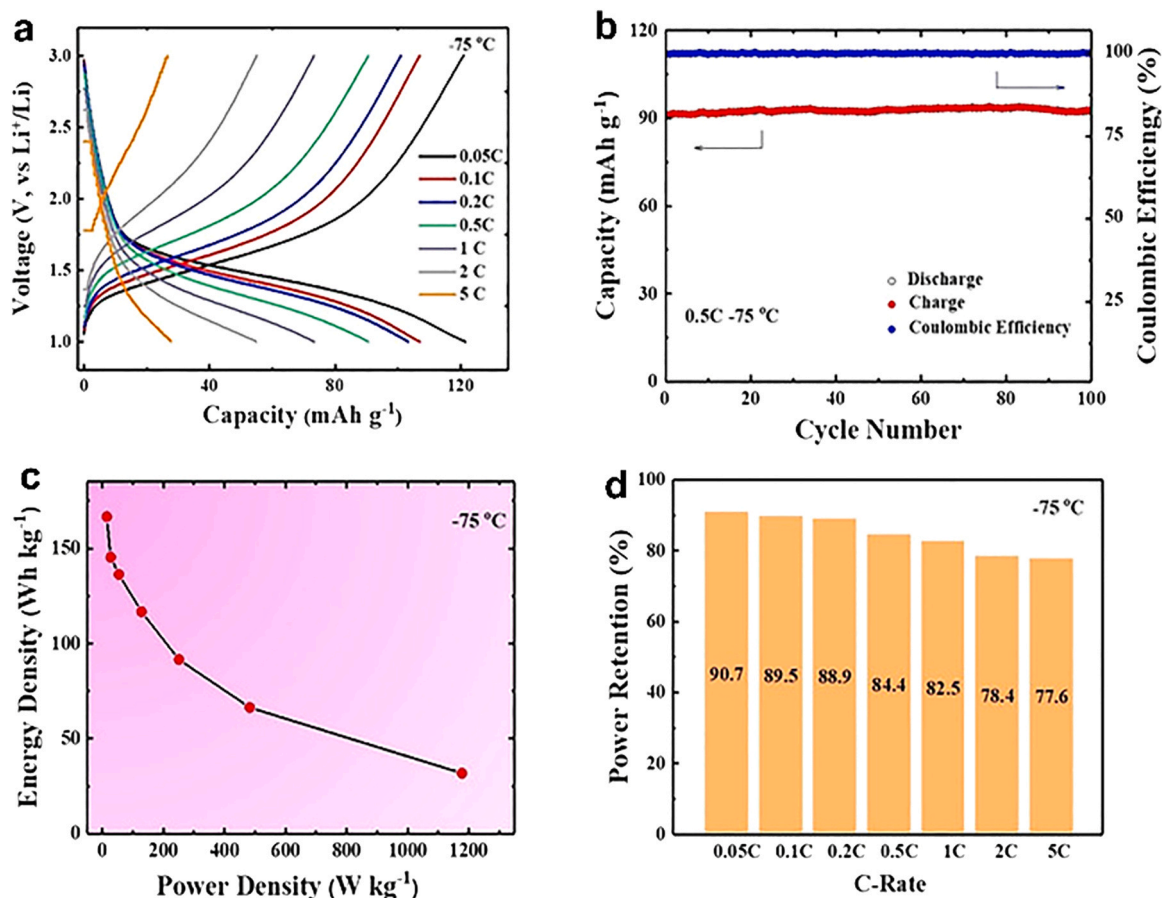


**Fig. 5.** Electrochemical performance of Nb<sub>2</sub>O<sub>5</sub> at low temperature. a Charge/discharge curves with various rates at -75 °C; b cycle performance with 0.5 C; c Ragone plot and d retention of the power density at -70 °C compared to that obtained at 25 °C.

capability and low-temperature electrochemical performance. From Fig. 6a and b, compared with nano-LMO, n-LG has only minor shape and platform position changes in the voltage curves at 25 °C, 0 °C, and -20 °C. This indicates that n-LG maintains faster kinetics at low temperature. In Fig. 6c, at -20 °C, the capacity retention of n-LG exceeds that of nano-LMO, even at 1 C, the capacity retention is 88%. In Fig. 6d, the impedance difference between nano-LMO and n-LG increases with the decrease in temperature, and the impedance of n-LG is smaller, which further indicates that the structure of nano-LMO and GNF promotes efficient charge transfer.

### 3. Cathode materials for sodium batteries

To date, a variety of alternative energy storage technologies with high energy density have emerged. In fact, rechargeable batteries used in electric vehicles not only need to provide high energy density but also need to be quickly charged and discharged in a wide temperature range. The application of lithium-ion batteries in electrical equipment is hindered by the shortage of lithium resources, and sodium-ion batteries are comparable to lithium-ion batteries in large-scale electrical energy storage while meeting the needs of the richness of sodium resources and the wide geographical distribution of sodium resources [103–105]. Therefore, considering the market and cost, sodium-ion batteries should be chosen to replace lithium batteries. Cathode materials used in sodium-ion batteries at low temperatures mainly include Prussian blue/Prussian blue analog cathodes, polyanion cathodes, and oxide cathodes. Unfortunately, these cathode materials are not perfect at low temperatures. The lack of sodium ion active sites in Prussian blue crystals results in a decrease in capacity [109]; the polyanion cathode has low operating voltage and low energy density;

the oxide cathode material may undergo a large number of side reactions, resulting in a change in the structure and volume of the material and a decrease in rate characteristics [125].

#### 3.1. Prussian blue and Prussian blue analogs cathode

Prussian blue is a low-cost cathode material with small volume changes during the cycle and high energy density. The open frame structure enables the Prussian blue compound to have long-period cycle stability and high-rate performance [106–108]. However, there are a large number of voids in the crystal structure of the Prussian blue compound synthesized by the traditional rapid precipitation method. These voids will be occupied by coordination water, resulting in the loss of sodium-ion storage active sites [109,110], and the reversibility of the material is reduced. However, this material has been extensively studied.

In order to make the Prussian blue electrode have excellent electrochemical performance at low temperature, Du et al. [111] investigated a solid polymer electrolyte (PFSA-Na membrane) for solid Na-ion batteries. In traditional liquid electrolyte batteries, the electrode-electrolyte interface is unstable due to the severe side reaction between the active material and the liquid electrolyte. In contrast, solid polymer electrolytes are only slightly polarized at low temperatures. They prepared solid-state sodium-ion batteries with PFSA-Na as the electrolyte and Prussian blue as the cathode. A strong interfacial layer is formed due to the stable interfacial compatibility between the PFSA-Na film and the Prussian blue electrode exhibited by the Na-ion battery. This modifies the deposition of sodium for good rate capability and long cycle life at room temperature and good electrochemical performance at low temperature. It can be seen from Fig. 7a that this solid-state Na-

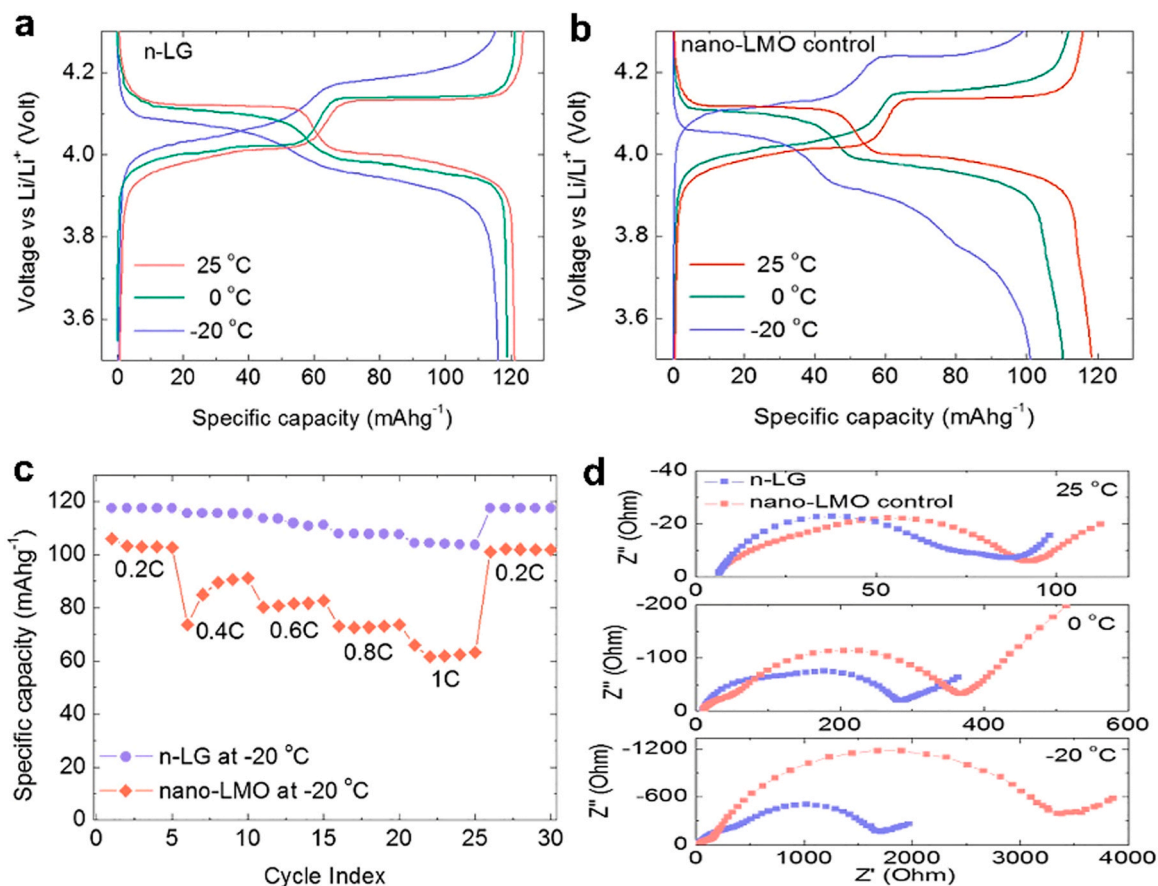


**Fig. 6.** Low temperature performance of n-LG cathode. a, b Voltage profiles of n-LG and nano-LMO control, respectively, with current rates of 0.2 C at 25 °C, 0 °C, and -20 °C; c Direct rate capability comparison between n-LG and nano-LMO at -20 °C; d Electrochemical impedance spectra of n-LG and nano-LMO control at 25 °C (top), 0 °C (middle), and -20 °C (bottom).

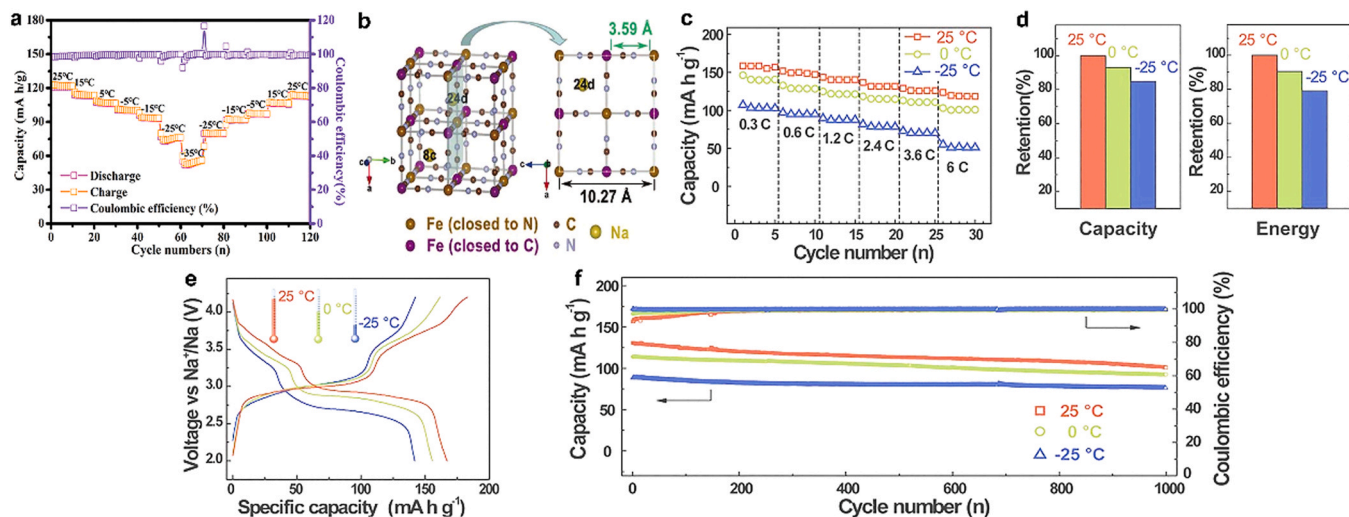


**Fig. 7.** a Low temperature cycling test of SSIBs. b The crystal structure of the PB obtained by DFT calculations, showing the possible Na<sup>+</sup> occupancy sites containing face-center (24d) and body-center site (8c), the crystal parameters, and the size of diffusion channels. c energy density and specific capacity retentions of the PB/CNT cathode at different temperatures; d Rate capabilities and e GDC profiles at 0.1 C. f extended cycling performance at 2.4 C of the PB/CNT cathode at different temperatures.

ion battery exhibits superior cycling performance even at a low temperature of -35 °C, far exceeding that of its liquid counterpart, with the coulombic efficiency maintained at 100%.

At low temperature, the contact between the active electrode particles and the current collector of Na-ion batteries is a concern, which can be solved by surface coating, doping with heteroatoms, etc.

You et al. [112] found that monodisperse Prussian blue nanocubes could nucleate on the carbon nanotube conductive network to form a robust and flexible composite cathode material PB/CNT. (C≡N)<sup>-</sup> increases the opening of perovskite framework faces, the small charge and triconium in the anion reduce the p-π interaction between Na<sup>+</sup> and anion [113]. It can be seen from Fig. 7b that in the

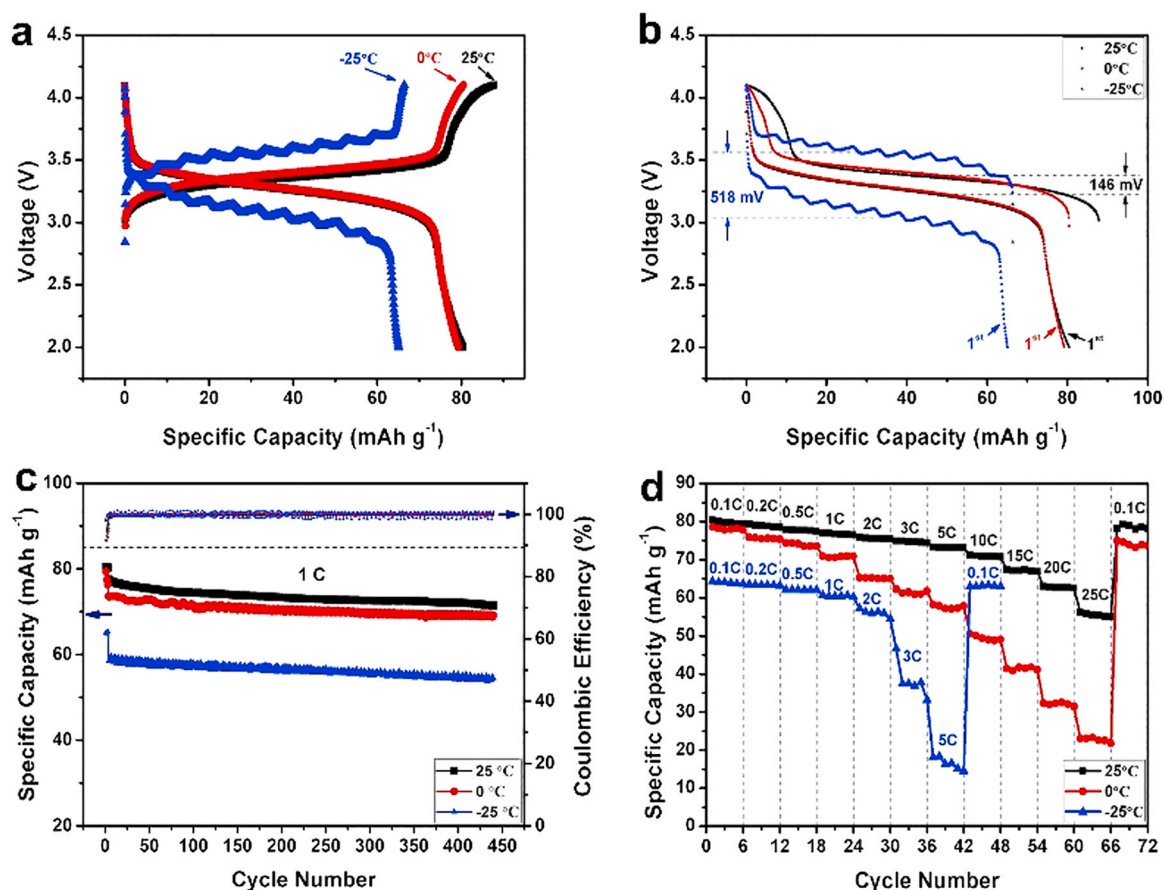


**Fig. 8.** Electrochemical properties of PBNI-ES at different temperatures: a the initial charge/discharge profiles at 0.1 C; b comparison of charge/discharge profiles; c cycle performance; d rate performance.

three-dimensional PB framework,  $\text{Na}^+$  has a larger ion diffusion channel with a channel diameter of 3.59 Å. Together with the weak interaction between  $\text{Na}^+$  and cyanide ions, it leads to the fast transport of  $\text{Na}^+$  within the reactive Prussian blue particles. In Fig. 7c, the PB/CNT cathode exhibits good rate capability over a wide temperature range, with a reversible capacity of  $88.4 \text{ mAh g}^{-1}$  at 2.4 C, which is 67% of the reversible capacity at 25 °C. In Fig. 7d, compared with 25 °C, the discharge capacity retention rate of the composite cathode at -25 °C can reach 85%, and the specific energy density can reach 79%. The galvanostatic charge-discharge voltage distribution of the half-cell using organic electrolyte at 0.1 C rate when the temperature is between -25 °C and 25 °C is shown in Fig. 7e. When PB/CNT is cycled at low temperature, its small volume change inhibits particle crushing and ensures good contact between CNT and PB crystals. As can be seen from Fig. 7f, at -25 °C, the PB/CNT composite cathode exhibits a fast and stable electrochemical cycling with a capacity retention of 86% after 1000 cycles at 2.4 C. Even at extremely low temperatures, the PB/CNT composites exhibit excellent low-temperature performance in terms of specific energy density, high rate capability, and long cycle life.

Based on the fact that the open crystal structure of Prussian blue is conducive to the migration of  $\text{Na}^+$  and can effectively adapt to the change of crystal volume, Ma et al. [114] proposed a new electrostatic spray-assisted coprecipitation (ESAC) method to synthesize  $\text{Na}_2\text{Ni}[\text{Fe}(\text{CN})_6]$  with Prussian blue structure. (PBNI-ES) cathode. The method avoids the existence of a large number of  $\text{Fe}(\text{CN})_6$  defects and coordination water in the crystal structure and effectively inhibits the growth rate of the crystal. This cathode material has ultra-high coulombic efficiency, good cycling performance, and rate capability. Fig. 8a compares the electrochemical performance of PBNI-ES

at different temperatures. At -25 °C, the initial discharge capacity of PBNI-ES is  $60 \text{ mAh g}^{-1}$ , which is shown as a waveform discharge curve. There may be two reasons for this. First, the PBNI-ES cathode is seriously polarized at low temperature, the internal resistance of the battery is large, and the voltage platform locally decreases; As the temperature rises, the PBNI-ES is partially activated and the voltage plateau rises. As the temperature increases, the internal resistance decreases, and the heat in the battery also decreases. As shown in Fig. 8b, the degree of polarization at -25 °C is significantly higher than that at 25 °C and 0 °C. In Fig. 8c, after 440 cycles at -25 °C, the capacity retention of PBNI-ES reaches 84% ( $54 \text{ mAh g}^{-1}$ ) and the coulombic efficiency is close to 100%. However, as can be seen from Fig. 8d, the rate performance of the PBNI-ES cathode deteriorates significantly at -25 °C. At 5 C, the discharge capacity at -25 °C is only 22% of that at 25 °C. This is mainly because the electrolyte freezes at low temperature and the conductivity decreases.

### 3.2. Polyanion cathode

Among all SIB cathode materials, polyanionic phosphates with NASICON crystal structures have received widespread attention due to their stable three-dimensional framework structure [115]. As a typical NASICON cathode, sodium vanadium phosphate ( $\text{Na}_3\text{V}_2(\text{PO}_4)_3$ ) has been extensively studied because its crystal lattice allows ultrafast and stable sodium insertion/extraction [116] and has high energy characteristics and excellent low-temperature performance. Unfortunately, its operating voltage is lower and its theoretical energy density is even lower than that of commercial lithium-

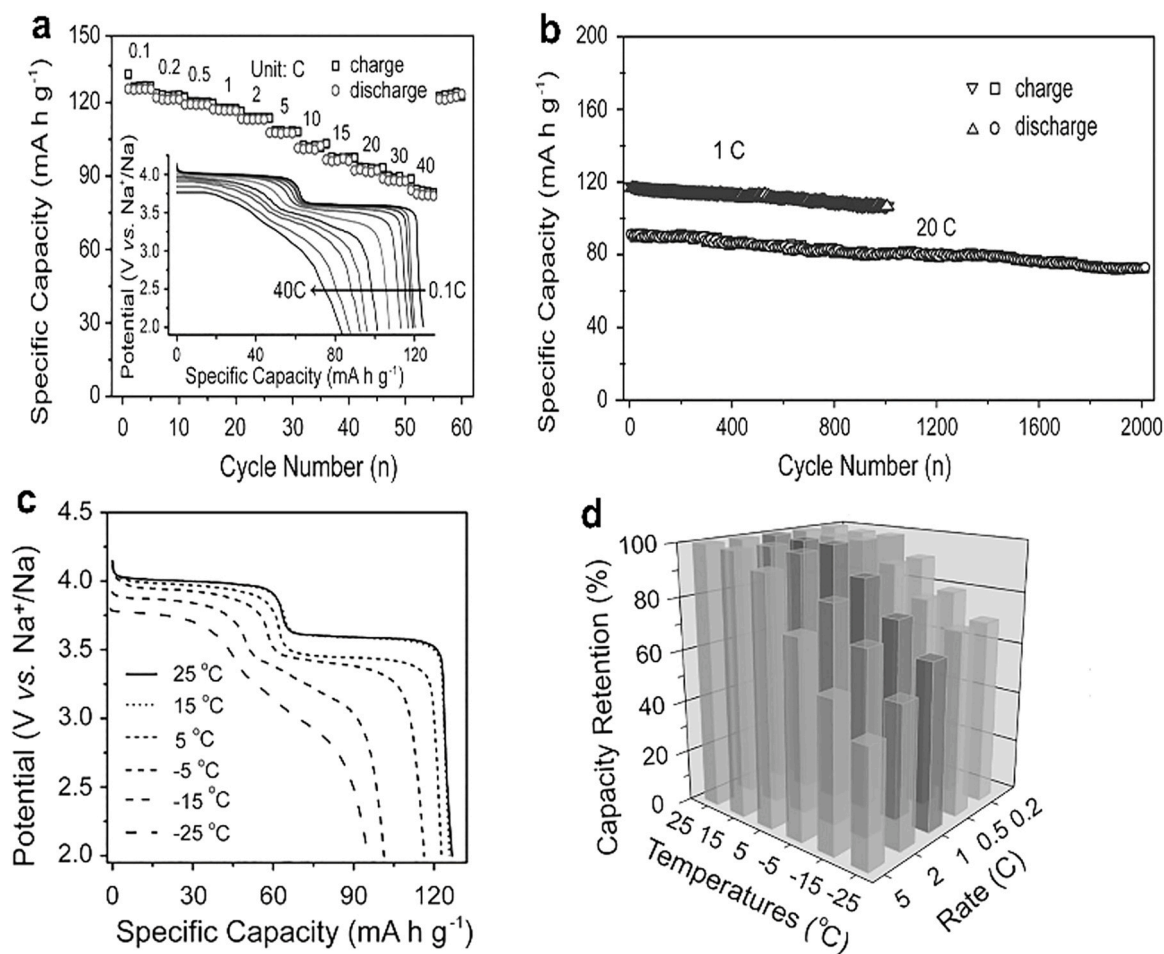


**Fig. 9.** a, b Electrochemical properties of NVPF-NTP in half cells: a Rate capabilities from 0.1 C to 40 C and the corresponding GCD curves (inset); b The cycle stabilities at different rates of 1 C for 1000 cycles and 20 C for 2000 cycles. c, d Low-temperature performance of NVPF-NTP: c Galvanostatic discharge curves of NVPF-NTP cycled at 0.2 C in the temperature range from 25 to -25 °C; d The capacity retentions along with temperature variations between 25 and -25 °C at various rates of 0.2, 0.5, 1, 2, and 5 C.

ion battery cathodes. Therefore, the low-temperature application of  $\text{Na}_3\text{V}_2(\text{PO}_4)_3$  in Na-ion batteries is hindered.

In order to improve the working voltage and energy density of  $(\text{Na}_3\text{V}_2(\text{PO}_4)_3)$ , researchers usually introduce highly electronegative anions (such as  $\text{F}^-$  and  $\text{O}^{2-}$ ) into the lattice to enhance the ionicity of the anion framework and shorten the  $\text{Na}^+$  diffusion pathway. After introducing  $\text{F}^-$  into the sodium phosphate lattice to form a new sodium fluorophosphate, the V-O bond is replaced by a V-F bond. In the process of sodium intercalation/extraction, the change of the valence state of V leads to higher redox potential. In addition, the lower the F content, the weaker the induction effect, which is beneficial to the diffusion of sodium and lower polarization at low temperature [117].

Guo et al. [118] prepared a  $\text{Na}_3\text{V}_2(\text{PO}_4)_2\text{O}_2\text{F}$  material composed of uniform and carbon-free nano-tetraprisms (NVPF-NTP) by a controlled hydrothermal method. When used as the cathode of SIBs, it has a long cycle life, an improved discharge platform, and an energy density increase of 23%, which is almost higher than that of all sodium-ion battery cathode materials. Fig. 9a shows the rate capability of NVPF-NTP at different discharge rates. Even when the discharge rate of the cathode material is 40 C, it only takes 90 s to complete the charge and discharge. Fig. 9b shows that 86% of the capacity can be maintained after 1000 cycles at a rate of 1 C, and 80.9% of the capacity can be maintained after 2000 cycles at 20 C. Fig. 9c shows the discharge curves at different test temperatures. In Fig. 9d, the capacity retention at different discharge rates and test temperatures is revealed. At a rate of 0.2 C, the capacity retention at -25 °C is more

than 76% compared to 25 °C. This shows that the NVPF-NTP electrode has good low temperature kinetics.

Guo et al. [119] assembled  $\text{Na}_3\text{V}_2(\text{PO}_4)_2\text{O}_2\text{F}$  and commercial graphite anodes into a new lithium/sodium-ion hybrid full battery (HNLIB). The hybrid battery has excellent rate capability and long-term cycle life. As shown in Fig. 10a, the assembled HNLIB battery has excellent high-rate performance in a wide current range of  $0.065\text{--}2.600\text{Ag}^{-1}$ , with a capacity retention rate of 66%. In Fig. 10b, after 2000 cycles, the capacity retention rate is still 86.3%. In addition, the HNLIB battery achieves excellent low temperature performance. Fig. 10c shows the GCD curve when the current density is  $0.013\text{Ag}^{-1}$  in the temperature range of 25 to -25 °C. Even at a low temperature of -25 °C, the capacity retention rate is 80.6%, and there are still two obvious platforms indicating that the assembled HNLIB battery has excellent low-temperature kinetics. In Fig. 10d, at -25 °C, after 100 cycles, the capacity retention rate is as high as 94.5%.

Wang et al. [120] prepared a high-voltage cathode  $\text{Na}_3\text{V}_2(\text{PO}_4)_2\text{O}_2\text{F}$  (NVPOF) and assembled it with a 3D Se/graphene (3DSG) composite anode to form a low-temperature sodium-ion full battery (SIFB). Fig. 11a shows the charging and discharging process of the battery. In Fig. 11b-c, the Ragone diagram of the 3DSG//NVPOF SIFB shows that compared with other products, the battery provides the highest energy and power density values. After 15,000 cycles, the capacity retention rate can still reach 86.3%, with high cycle stability and long cycle life. Fig. 11d-f shows that the 3DSG//NVPOF SIFB has excellent low temperature performance. At a temperature of 25 °C to -25 °C, after 1000 cycles at  $0.4\text{Ag}^{-1}$ , the capacity retention rate is

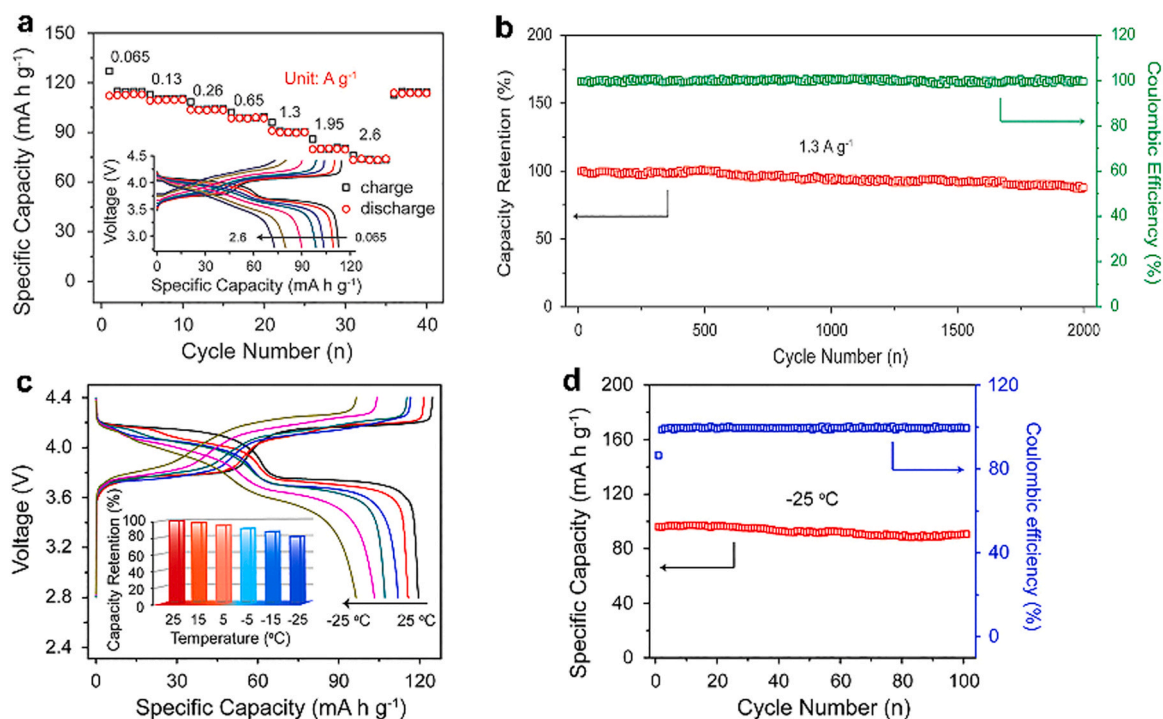


**Fig. 10.** Electrochemical performance of the assembled MCMB//NVPOF HLNIBs. a Rate capability and the corresponding GCD curves (inset) at various current densities from 0.065 to 2.6 A g<sup>-1</sup>; The cycling performances at current densities of b 1.3 A g<sup>-1</sup> over 200 and 2000 cycles. c The GCD curves and capacity retention (inset) cycled at 0.013 A g<sup>-1</sup> in the temperature range from 25 to -25 °C; d Cycling performance at 0.013 A g<sup>-1</sup> under -25 °C over 100 cycles.

greater than 75%. Fig. 11e further shows the diagram at different temperatures, revealing that the 3DSG//NVPOF SIFB has low-temperature dependence and good low-temperature performance.

### 3.3. Oxide cathode

At low temperatures, the limitations of sodium-ion batteries may be attributed to the low conductivity of the electrolyte, the high barrier of Na<sup>+</sup> desolvation in the electrode/electrolyte interface, and the slow sodium transport kinetics [121,122]. The aforementioned Prussian blue/Prussian blue analogs and Na<sub>3</sub>V<sub>2</sub>(PO<sub>4</sub>)<sub>2</sub>O<sub>2</sub>F with sodium superion conductor crystal structures, and are the first choice for sodium-ion battery applications at low temperatures. However, due to the lack of

strict synthesis methods and theoretical capacity limitations, its commercial low-temperature applications are hindered. P2-type manganese-based layered oxide is an important cathode material, with a high theoretical capacity and a compact structure [123,124]. However, it will produce a large number of side reactions at the cathode-electrolyte interface, resulting in the reduction of Mn<sup>4+</sup> and the formation of an ionic insulating layer. The reduction of transition metals also induces the Jahn-Teller twist of Mn<sup>3+</sup>, which leads to volume change, structural disintegration, and metal dissolution. The migration of dissolved metal cations into the electrolyte interferes with the formation of a stable cathode-electrolyte interface, which in turn leads to a dramatic drop in discharge capacity [125,126]. In addition, the ionic insulating layer on the cathode surface hinders the

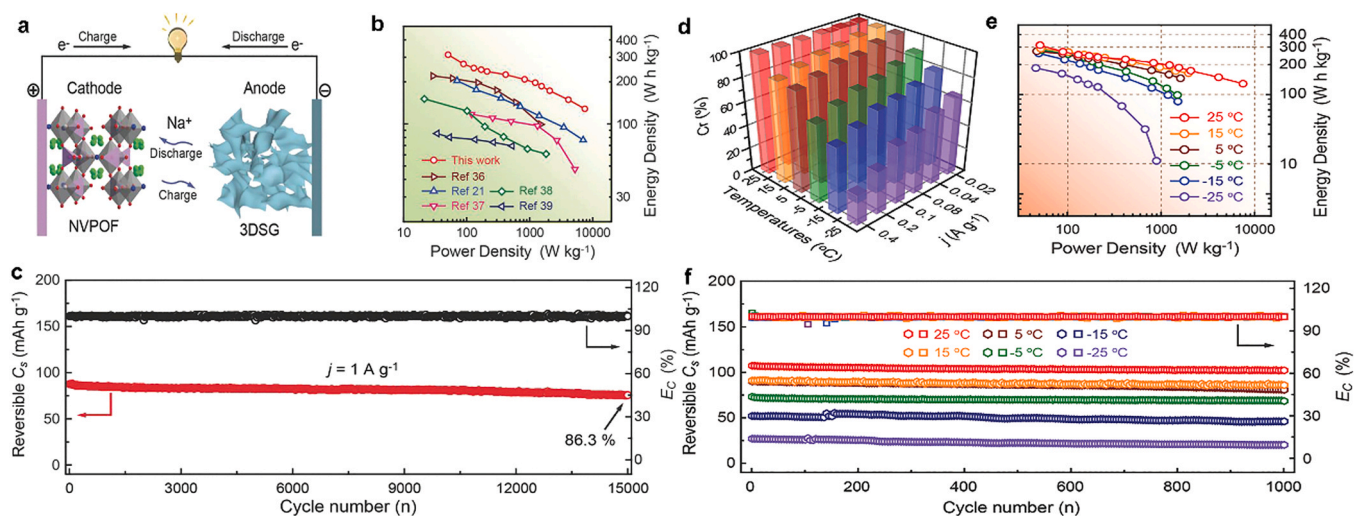


**Fig. 11.** Energy-storage performances of the 3DSG//NVPOF SIFB. a Schematic showing the charge/discharge processes; b Comparison of full-cell Ragone plots between 3DSG//NVPOF and other SIFBs reported previously, and c cycling performance at room-T and 1 A g<sup>-1</sup> after a rate test of 20 cycles. Low-T performance of the 3DSG//NVPOF SIFBs; d The Cr variations along with j and temperature tested; e Ragone plots and f cycling performance at 0.4 A g<sup>-1</sup> at varied temperatures from room-T to -25 °C.

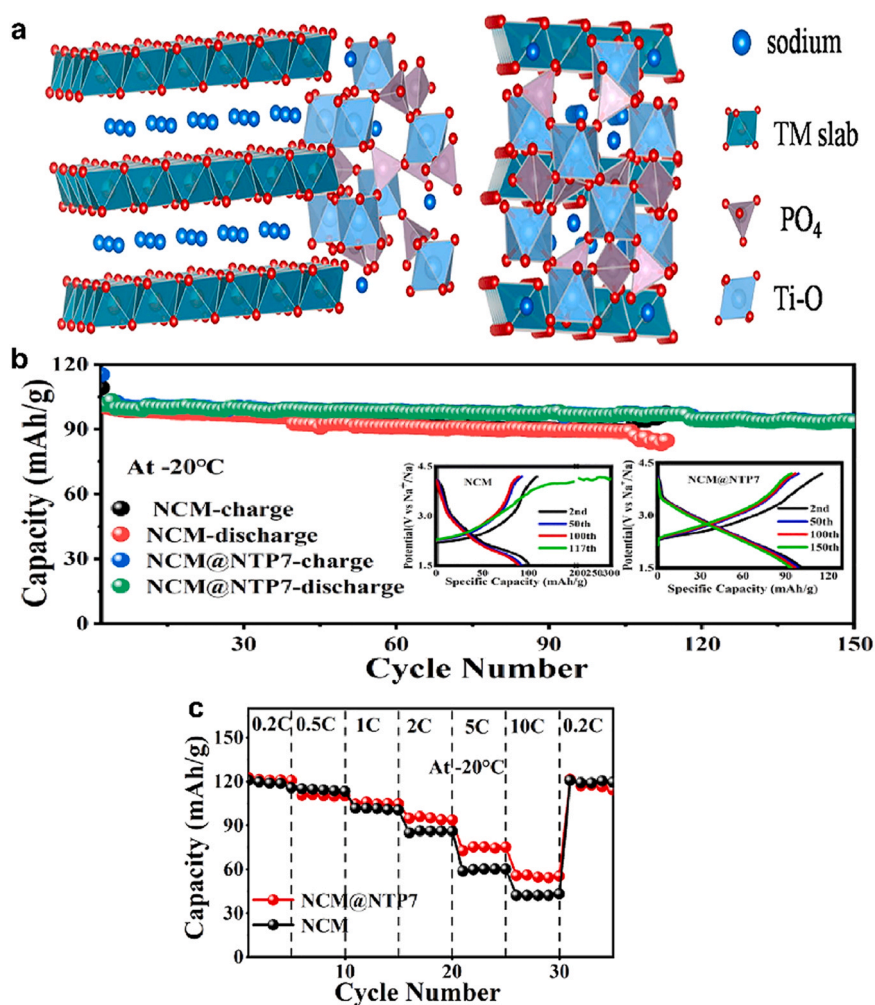


**Fig. 12.** Sodium storage properties of the pristine NCM and the NCM materials coated with different contents of NTP: a The interface model of NCM@NTP7 material; b Rate capabilities from 0.2C to 10C at  $-20^{\circ}\text{C}$ ; c Cycle performances at 0.5C for 150 cycles at  $-20^{\circ}\text{C}$ .

diffusion channel of sodium, increases the diffusion barrier and charge transfer resistance of sodium, and inhibits its rate characteristics [127,128]. Therefore, its electrochemical performance at low temperature is also severely hindered. In order to have excellent low-temperature electrochemical performance, a reasonable reconstruction of the material surface is required.

Li et al. [129] designed a Nasicon-type  $\text{NaTi}_2(\text{PO}_4)_3$  (NTP) nanoshell, which was coated on the surface of a  $\text{Na}_{0.67}\text{Co}_{0.2}\text{Mn}_{0.8}\text{O}_2$  (NCM) host through the combination of conventional wet coating and solid-phase reaction. They successfully synthesized NCM@NTP7 cathode and its interface model is shown in Fig. 12a. This NTP nanoshell coating alleviates the phase transition on the NCM surface, suppresses the Jahn-Teller deformation and metal dissolution, and has a good protective effect on the cathode. The transfer kinetics and structural stability of sodium ions are significantly improved by hindering the direct contact between the electrolyte and the host material. As shown in Fig. 12b, at a low temperature of  $-20^{\circ}\text{C}$ , NCM@NTP7 has a higher discharge capacity with an increasing discharge rate. As shown in Fig. 12c, NCM@NTP7 exhibited superior cycling stability compared with NCM after 150 cycles.

In addition, Li et al. [130] proposed a P2-type  $\text{Na}_{0.67}\text{Ni}_{0.1}\text{Co}_{0.1}\text{Mn}_{0.8}\text{O}_2$  (NMCM) cathode material. The partial substitution of Co/Ni with similar ionic radii and different redox potentials can effectively shield the electrostatic interaction of  $\text{Na}^+$ /vacancy order, expand the Na layer distance from the shrinkage of the transition metal dioxide flat plate, and improve the electrochemical reaction kinetics at low temperature.

The cathode material has an excellent  $\text{Na}^+$  diffusion coefficient at  $-20^{\circ}\text{C}$ , and the structural stability is increased. It can be seen from the constant current charge-discharge curve in Fig. 13a at  $-20^{\circ}\text{C}$ , that the voltage plateau of the (P2- $\text{Na}_{0.67}\text{MnO}_2$ ) NM sample is complicated, and the curve corresponding to NMCM is a diagonal line. NMCM exhibits ultrahigh-specific capacity at low temperatures. This high-performance result effectively inhibits the orderly rearrangement and phase transition of  $\text{Na}^+$ /vacancies. As shown in Fig. 13b, at a low temperature of  $-20^{\circ}\text{C}$ , the discharge capacity of NMCM at 1, 5, and  $10^{\circ}\text{C}$  exceeds that of NM and some previously reported sodium cathode materials. In Fig. 13c, transport kinetics were assessed by electrochemical impedance spectroscopy (EIS). When the temperature dropped to  $-20^{\circ}\text{C}$ , the NMCM electrode exhibited lower charge transfer resistance, providing stable desolvation and higher electroactivity, indicating its higher low-temperature rate capacity and cycling stability. In Fig. 13d, the NMCM showed high capacity retention of 80% after 300 cycles at a low temperature of 1C. Fig. 13e demonstrates the sodiation of NMCM electrodes. Disordered Na vacancies lead to solid solution reactions in bulk electrodes, and pseudocapacitive properties facilitate  $\text{Na}^+$  desolvation at the electrolyte/electrode interface, resulting in a high electrochemical performance at low temperature.

#### 4. Cathode material for magnesium-ion battery

Magnesium-ion batteries are considered to be an attractive technology due to their high natural magnesium content, large

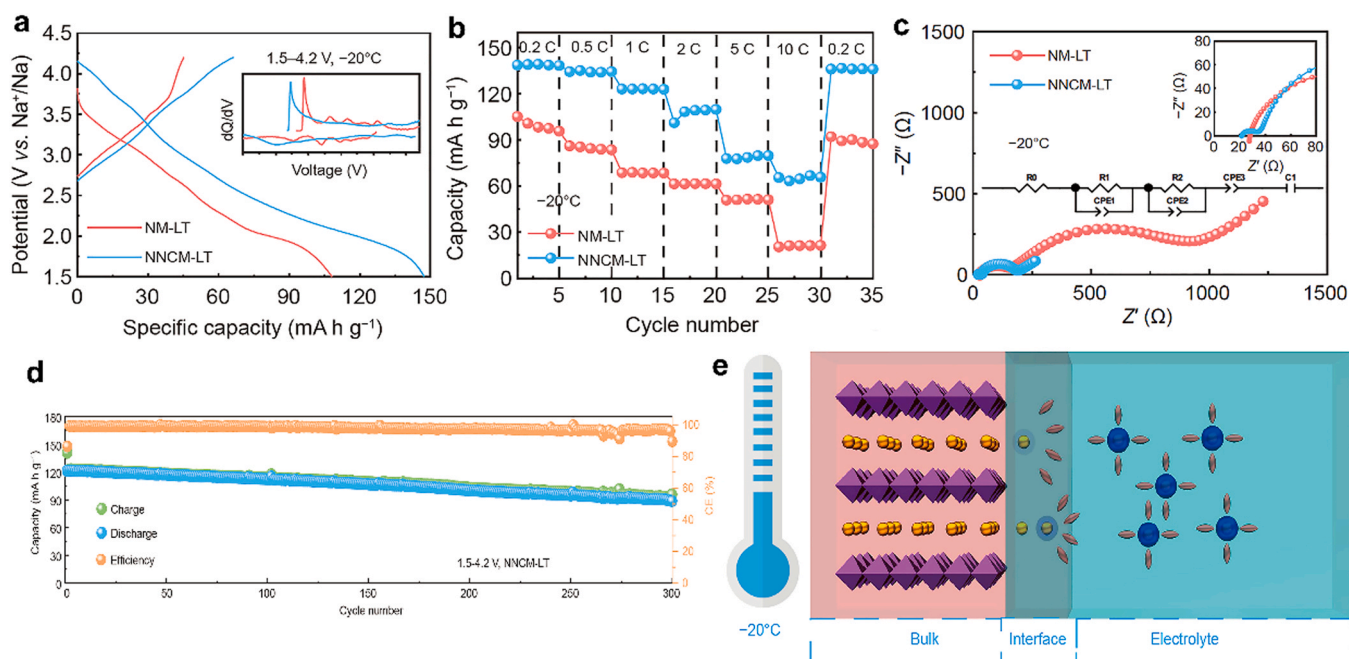


**Fig. 13.** a Galvanostatic charge-discharge curves and  $dQ/dV$  profiles (illustration) of the NNCM electrode at  $-20^\circ\text{C}$  and 0.2C; b Rate capabilities at different rates; c EIS curve of NNCM-LT electrodes; d Long-term cycle performance of NNCM-LT at 1C; e Sodiation with the synergistic effect of the surface-controlled intercalation pseudocapacitive behavior at the interface and high diffusion coefficient in the bulk electrode.

theoretical capacity, and lack of a dendritic cycle. To bypass the slow transmission of magnesium ions and make full use of the dendritic-free cycle of magnesium metal anodes, the concept of hybrid ion batteries has emerged as a new strategy in recent years [131]. High-performance rechargeable magnesium-ion batteries have become potential candidates for the next generation of new batteries due to their unique advantages [132]. In extremely low temperature environments, polyanionic materials and oxides are commonly used as cathode materials for magnesium-lithium mixed-ion batteries. However, the former has the problems of slow ion transfer, poor electrical conductivity, and a significant drop in capacity [63], and the latter cannot perform well at low temperatures due to poor electrical conductivity [142].

#### 4.1. Polyanion cathode

The polyanion  $\text{LiFePO}_4$  (LFP) cathode has the advantages of moderate operating voltage, large capacitance, high discharge power, fast charging and long cycle life. However, there are problems of slow ion diffusion, poor electrical conductivity, and decreased capacity, which seriously hinder their performance at low temperatures. (detailed in Section 2.1). Research on magnesium-ion batteries at low temperatures is mostly based on mixed ion electrolytes. Zhang et al. [133] used a flexible pyrolytic graphite film (GF) as a reliable high-voltage cathode current collector and selected a relatively high-voltage  $\text{LiFePO}_4$  cathode as shown in Fig. 14a. Metal magnesium was used as an anode, dissolved in tetrahydrofuran (THF) solvent aluminum chloride ( $\text{AlCl}_3$ ), and phenyl magnesium chloride ( $\text{PhMgCl}$ ) salts were prepared to prepare all-phenyl complex (APC) electrolytes, and the ultralow temperature performance of magnesium-lithium hybrid ion batteries was studied. It is found by cyclic voltammetry that as the concentration of lithium-ions increases, the current intensity of both the cathode and anode increases. The optimized electrolyte solution can be used for room temperature and ultralow temperature electrochemical characterization. Fig. 14b shows that after 200 cycles at room temperature, the capacity drops to  $102.4\text{mAhg}^{-1}$ , and the retention rate is 98.5%. As shown in Fig. 14c, the higher the current density, the lower the

specific capacity. Compared with magnesium batteries, the operating voltage of hybrid batteries is significantly improved. At low temperature, due to the low viscosity and low melting point of the THF solvent in the electrolyte, it can resist the freezing of the solution, so the hybrid ion battery has excellent electrochemical performance at ultra-low temperature. The  $\text{LiFePO}_4$  cathode batteries were tested at 0,  $-10$ ,  $-20$ , and  $-40^\circ\text{C}$ . After analyzing Fig. 14d-e, it was found that the maximum capacity of the magnesium-lithium mixed-ion battery and pure lithium-ion battery at  $0^\circ\text{C}$  was  $103.5\text{mAhg}^{-1}$  and  $109.8\text{mAhg}^{-1}$ , respectively. When the mixed-ion battery was at 0,  $-10$ ,  $-20$ , and  $-40^\circ\text{C}$ , its reversible capacities reached 109, 100, 90, 90 and  $80\text{mAhg}^{-1}$ , respectively, without capacity-fading.

The polyanionic material  $\text{Li}_3\text{V}_2(\text{PO}_4)_3$  (LVP) has become an efficient cathode material for LIBs due to its abundance, high safety, and high theoretical capacity [134]. However, due to polarization, the anions and cations move toward the positive and negative electrodes, respectively, during the charging and discharging process, and lithium is deposited on the negative electrode. Inhomogeneous Li deposits continue to occur upon cycling at high current densities, and these Li deposits grow as dendrites, resulting in volume expansion that eventually punctures the separator [135]. This will inevitably have an impact on the performance of LVP-based lithium-ion batteries. This can lead to low energy density, short cycle life, and short-circuiting of the battery, eventually leading to fire or other hazards [136]. In order to make full use of the potential of LVP cathode and avoid the problem of dendrite growth and apply it in  $\text{Mg}^{2+}/\text{Li}^+$  mixed-ion batteries, choosing a suitable electrolyte is a good strategy. Rashad et al. [137] applied polyanionic  $\text{Li}_3\text{V}_2(\text{PO}_4)_3$  (LVP) cathodes to magnesium-lithium mixed-ion batteries (MLIBs) to evaluate their room temperature and ultralow temperature performance. They studied two different magnesium electrolytes (all-phenyl-complex, magnesium boro-hydrides in diglyme) and inorganic lithium additives. By comparing the rate performance of LVP/APC-LiCl/Mg and LVP/Mg/Li-BH/Mg batteries at room temperature, they found that the APC-LiCl/THF electrolyte has excellent rate performance and high specific capacity. As shown in Fig. 14f-i, the half-cell is transferred to a low temperature and

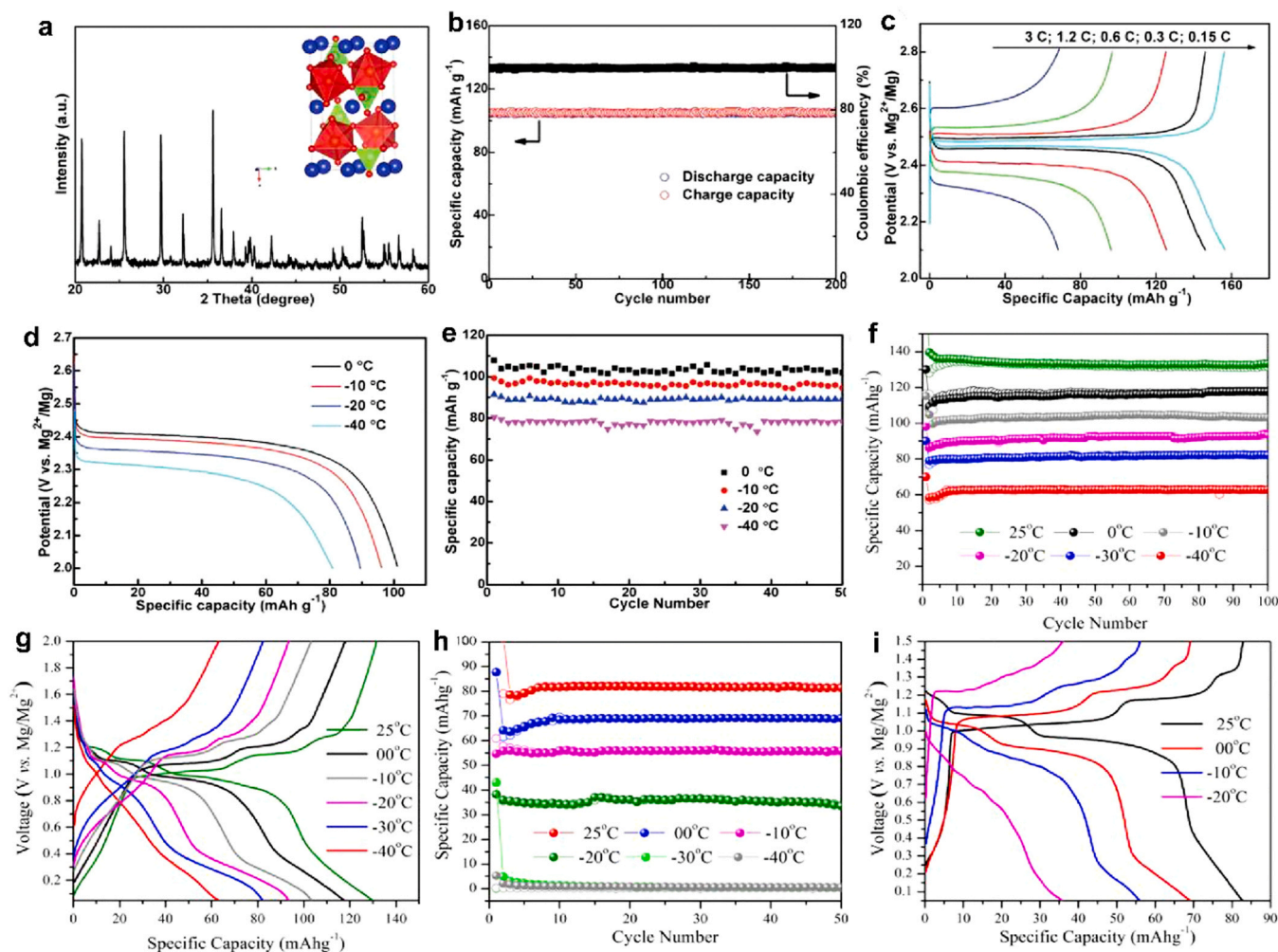


**Fig. 14.** a XRD pattern of the commercial LFP powder (inset: crystal structure of LFP); b Discharge-charge cycling performance and the corresponding coulombic efficiency of the LFP@GF electrode for hybrid  $\text{Mg}^{2+}/\text{Li}^+$  batteries at room temperature; c Galvanostatic discharge-charge profiles of the rate performance at various rates, galvanostatic discharge-charge profiles d and cycling performance e of the hybrid  $\text{Mg}^{2+}/\text{Li}^+$  battery at various low temperatures. f Cycle performance of LVPI/APC-LiCl|Mg cells at RT and low temperatures (0, -10, -20, -30, and -40 °C) at  $100\text{mA g}^{-1}$  current rate; g Corresponding charge-discharge curves; h Cycle performance of LVPI|Mg/Li-BH|Mg cells at RT and low temperatures (0, -10, -20, -30, and -40 °C) at  $100\text{mA g}^{-1}$  current rate, and i Corresponding charge-discharge curves.

subjected to 100 cycles at 25, 0, -10, -20, -30, and -40 °C to obtain reversible capacities of 135, 117, 103.5, 93.4, 82.2, and  $63.1\text{mAh g}^{-1}$  respectively. At the same time, it can be observed that the voltage plateau decreases with decreasing temperature, but the battery still maintains its initial capacity, which reveals the high performance of the APC-LiCl-based electrolyte in low-temperature applications. LVP||APCLiCl|| after 50 cycles at -40 °C ultralow temperature, the reversible capacity remains unchanged, showing good electrochemical performance. This work shows that low-boiling electrolyte solutions are ideal devices for use at ultra-low temperatures.

At ultralow temperatures, polyanionic materials such as  $\text{LiFePO}_4$  and  $\text{Li}_3\text{V}_2(\text{PO}_4)_3$  have been widely used in rechargeable magnesium-ion batteries. Among them, lithium iron phosphate can use an APC-LiCl/THF-based electrolyte to produce acceptable energy density at a temperature of -40 °C.

#### 4.2. Oxide cathode

Layered vanadium oxides have attracted extensive research in the field of Li-ion intercalation due to their large specific capacity [138]. And vanadium oxides are abundant and cheap. Among them,  $\text{H}_2\text{V}_3\text{O}_8$ , as an important member, has a large interlayer distance between the  $\text{V}_3\text{O}_7$  layers by hydrogen bonds. These hydrogen bonds can alleviate

the structural changes during ion insertion/extraction without destroying the crystal structure [139]. In addition, the mixed valence of vanadium can optimize the electronic conductivity and provide more redox sites [140]. Therefore,  $\text{H}_2\text{V}_3\text{O}_8$  with the above characteristics is expected to become a high-performance cathode for magnesium-ion batteries at low temperatures. Tang et al. [141] investigated the electrochemical performance of  $\text{H}_2\text{V}_3\text{O}_8$  nanowires in magnesium-based batteries. Studies have shown that this cathode material has a high voltage platform of 2.0 V and a high specific capacity of  $304.2\text{mAh g}^{-1}$  at  $50\text{mA g}^{-1}$ , showing excellent electrochemical performance in magnesium batteries. Under the condition of  $100\text{mA g}^{-1}$  at -20 °C,  $\text{H}_2\text{V}_3\text{O}_8$  provided a specific capacity of  $34.5\text{mAh g}^{-1}$ .

The transition metal oxide lithium titanate ( $\text{Li}_4\text{Ti}_5\text{O}_{12}$ ) with a spinel structure is considered to be an ideal material due to its almost unchanged skeleton during charging and discharging, low operating potential, high coulomb efficiency, and high lithium-ion diffusion coefficient [142]. However, its poor electrical conductivity limits practical applications. Fortunately, its charge-discharge potential is in the range of magnesium electrolyte, so it can be used as a positive electrode for magnesium or magnesium-lithium mixed-ion batteries.

Rashid et al. [143] used lithium titanate cathodes, magnesium anodes, and all-phenyl complex electrolytes supplemented with

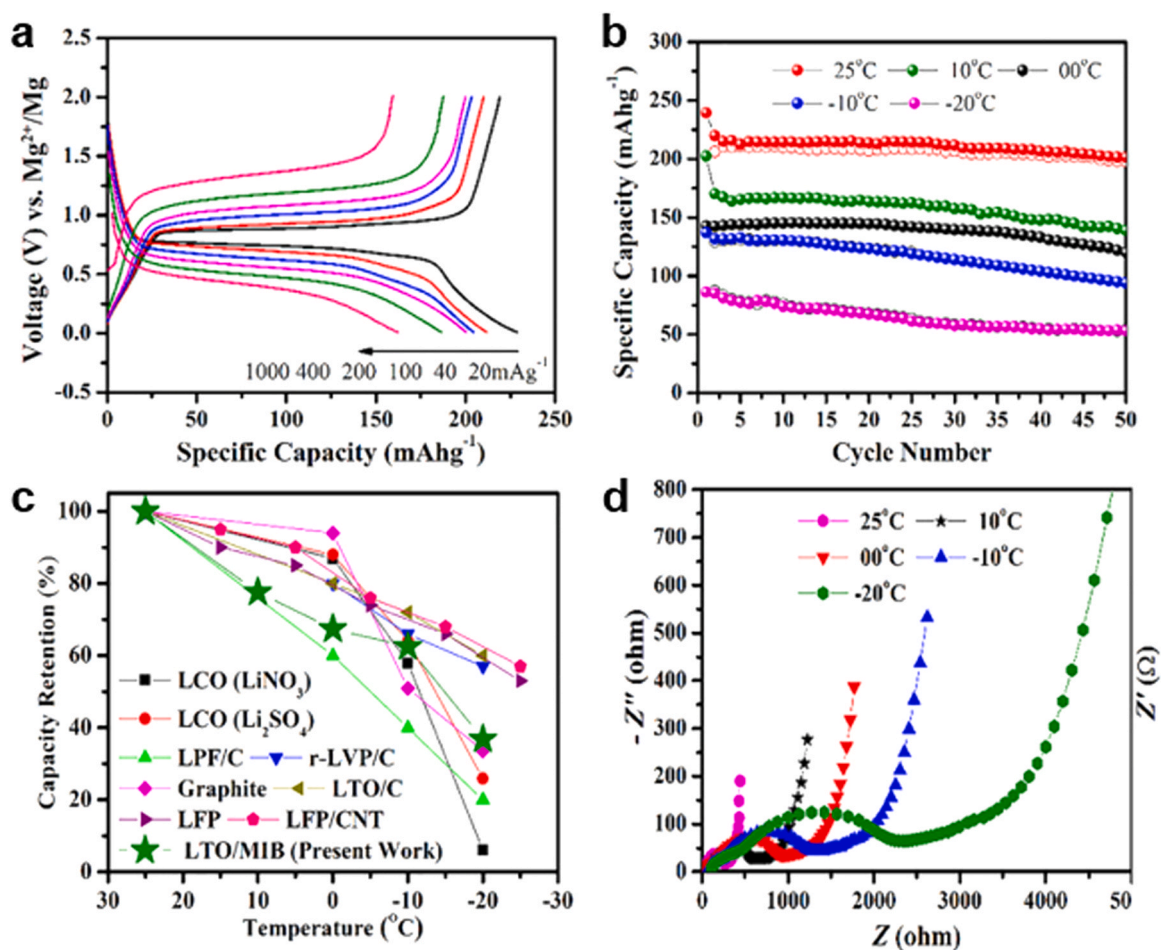


**Fig. 15.** a Galvanostatic charging-discharging curves at different current densities (20–1000 mA h<sup>-1</sup>) measured at room temperature (25 °C); b cycle stabilities of half-cells measured at different temperatures (25, 10, 0, -10, and -20 °C); c comparison of capacity retentions of present work with conventional LIBs tested at low temperatures; d Electrochemical impedance spectroscopy of LTO battery in 0.4 APC-1.0 LiCl electrolyte at different temperatures.

lithium salts to assemble magnesium-lithium mixed-ion batteries and analyzed their electrochemical performance at different temperatures. As shown in Fig. 15a-b, when the current density of the LTO cathode is 20, 40, 100, 200, 400, and 1000 mA h<sup>-1</sup>, the reversible capacity reaches 228, 212.5, 204.1, 199.7, 185.3, and 163 mA h<sup>-1</sup>, respectively. The discharge curve has a stable voltage platform. The half-cells underwent 50 cycles at different temperatures. The decrease in temperature reduces the capacity at 10 °C, 0 °C, -10 °C, and -20 °C by 22.4%, 32.6%, and 37.5%, respectively. In addition, 63.2%. The reason for this is the slower guest ion transport, which leads to the reduced diffusion of guest ions in the LTO cathode. Fig. 15c compares the capacity retention of MLIB and previously reported lithium batteries at different temperatures, and found that the lithium titanate cathode and APC-LiCl/THF electrolyte have excellent electrochemical performance at low temperature. This is because the APC-THF solution has a strong potential to inhibit the freezing of the electrolyte solution due to the lower boiling point of THF. To investigate the effect of temperature on cell resistance, half-cells at 25, 10, 0, -10, and -20 °C were tested by electrochemical impedance spectroscopy (EIS) in Fig. 15d. The values of ohmic resistance ( $R_{SEI}$ ), charge transfer resistance ( $R_{CT}$ ), and Warburg factor increased significantly with decreasing temperature.

## 5. Cathode materials for zinc-ion batteries

Zinc-ion batteries are characterized by low redox potential, high theoretical specific capacity, and high energy density [144–146].

However, due to the large atomic mass of zinc ions, the electrostatic capacitance interaction between them and the host lattice is strong, which leads to sluggish diffusion kinetics and poor rate performance [147,148]. The development of cathode materials for zinc ion batteries has also been deeply this effect. At low temperatures, researchers have studied oxides, metal salts, and organic cathodes and found that oxide cathodes have low ion transfer kinetics and poor rate performance; metal salt cathodes have a low capacity [163].

### 5.1. Oxide cathode

In recent years, vanadium-based composite materials have been extensively studied. Because of its high theoretical specific capacity, vanadium oxide is considered to be a very promising cathode material for zinc-ion batteries [149–152]. Its layered structure of vanadium pentoxide has been proven to be used as a cathode for zinc-ion batteries [153,154]. However, there are disadvantages such as low ion transfer mechanics, poor rate performance, and structural instability, which are further exacerbated at low temperatures. To improve the structural stability, electrochemical performance, and electrochemical reaction kinetics, the researchers optimized the zinc ion storage properties of V<sub>2</sub>O<sub>5</sub>. Geng et al. [155] used microwave-assisted synthesis of Mn<sup>2+</sup>-doped hydrated layered vanadium oxide (Mn<sub>0.15</sub>V<sub>2</sub>O<sub>5</sub>·nH<sub>2</sub>O). Through interlayer doping of Mn<sup>2+</sup> ions and water molecules to reduce the interlayer spacing, the unique nanostructure facilitates the penetration of electrolytes and the migration of Zn<sup>2+</sup>. The synergistic effect of the two can enhance the

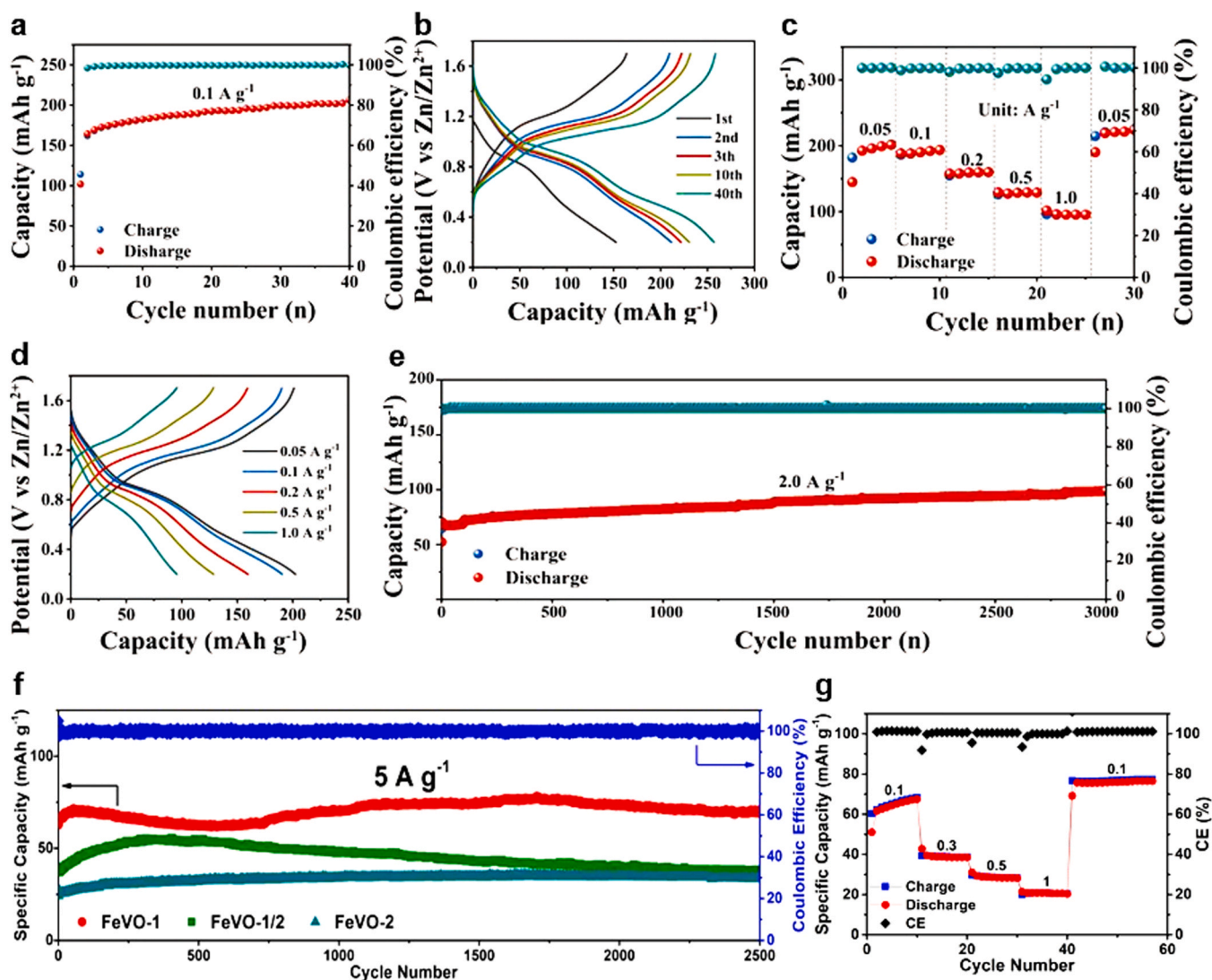


**Fig. 16.** Zinc-ion storage performance of the  $\text{Mn}_{0.15}\text{V}_2\text{O}_5 \cdot n\text{H}_2\text{O}$  electrode at a low temperature of  $-20^\circ\text{C}$ : a cycling performance at  $0.1\text{A g}^{-1}$  and b the corresponding galvanostatic charge-discharge profiles; c Rate capacities at current densities and d the corresponding charge-discharge profiles; e Long cycling performance at  $2.0\text{A g}^{-1}$ . f Long-term cycle performance of FeVO-1, FeVO-1/2, and FeVO-2 at  $5\text{A g}^{-1}$ ; g Rate performance of FeVO-1 at a low temperature of  $-20^\circ\text{C}$ .

electrical conductivity, ionic mobility, and structural stability of layered  $\text{V}_2\text{O}_5$  at low temperature. When  $\text{Mn}_{0.15}\text{V}_2\text{O}_5 \cdot n\text{H}_2\text{O}$  is used as the cathode, it exhibits ultra-high specific capacity, high current density, superior rate performance, and long-cycle stability. As shown in Fig. 16a-e, the  $\text{Mn}_{0.15}\text{V}_2\text{O}_5 \cdot n\text{H}_2\text{O}$  electrode exhibits a high reversible specific capacity of  $257\text{mAh g}^{-1}$  after 40 cycles at a low temperature of  $-20^\circ\text{C}$  and a current density of  $0.1\text{A g}^{-1}$ . As the current density decreased to  $0.05\text{A g}^{-1}$ , the specific capacity recovered to a higher value, indicating that the  $\text{Zn}^{2+}$  deintercalation/intercalation process is highly reversible. In addition, at a high current density of  $2.0\text{A g}^{-1}$ , the  $\text{Mn}_{0.15}\text{V}_2\text{O}_5 \cdot n\text{H}_2\text{O}$  material can also reach a high specific capacity of  $100\text{mAh g}^{-1}$  after 3000 cycles, which makes the  $\text{Mn}_{0.15}\text{V}_2\text{O}_5 \cdot n\text{H}_2\text{O}$  material more suitable for practical applications.

Luo et al. [156] used a hydrothermal method to synthesize amorphous  $\text{FeVO}_4$  with a hydrangea-like structure as a cathode for aqueous zinc batteries through rational bimetal design. This bimetallic Fe-V-O oxide exhibits strong electrode kinetics, which is attributed to the better electronic conductivity of Fe-V-O oxide than pristine  $\text{V}_2\text{O}_5$  due to the introduction of Fe element and amorphous crystal structure. It can provide reduced diffusion paths and larger free volume for  $\text{Zn}^{2+}$  insertion. Furthermore, the ultrathin  $\text{FeVO}_4$  nanosheets self-assemble into  $\text{FeVO}_4$  spheres like petals. This

biomimetic design not only expands the contact area between the electrolyte and the cathode but also effectively maintains the structural integrity during cycling. Therefore, it can be seen from Fig. 16f that the as-prepared  $\text{FeVO}_4$  exhibits long cycle stability with a discharge capacity of  $70\text{mAh g}^{-1}$  after 2500 cycles at a high current density of  $5\text{A g}^{-1}$ . Most importantly,  $\text{FeVO}_4$  still provides a considerable discharge capacity of  $80\text{mAh g}^{-1}$  at a current density of  $0.1\text{A g}^{-1}$  at a low temperature of  $-20^\circ\text{C}$  in Fig. 16g.

Zhang et al. [157] designed an electrolyte/cathode strategy to synthesize  $\text{Zn}||\text{V}_2\text{O}_5$  low-temperature aqueous zinc batteries. By using  $\text{Zn}^{2+}$  salt and  $\text{CF}_3\text{SO}_4^-$  to break the hydrogen bond in water and lower its freezing point to  $-34.1^\circ\text{C}$ , the  $\text{Zn}||\text{V}_2\text{O}_5$  battery works well at low temperature. The  $\text{V}_2\text{O}_5$  cathode has excellent capacity at low temperature, which is benefited from the kinetics of fast insertion of hydrated ions. The researchers assembled  $\text{Zn}||\text{V}_2\text{O}_5$  batteries containing  $\text{ZnSO}_4$  and  $\text{Zn}(\text{CF}_3\text{SO}_4)_2$  electrolytes and tested them at different temperatures from  $25$  to  $-30^\circ\text{C}$ , as shown in Fig. 17a-c. The results showed that the battery containing the  $\text{ZnSO}_4$  electrolyte had problems at  $-30^\circ\text{C}$ , while the battery containing the  $\text{Zn}(\text{CF}_3\text{SO}_4)_2$  electrolyte could still work normally. This shows that the role of unfrozen electrolyte is very important. At low current densities of  $0.1$  and  $0.5\text{A g}^{-1}$ , the battery containing  $\text{Zn}(\text{CF}_3\text{SO}_4)_2$  electrolyte and  $\text{V}_2\text{O}_5$

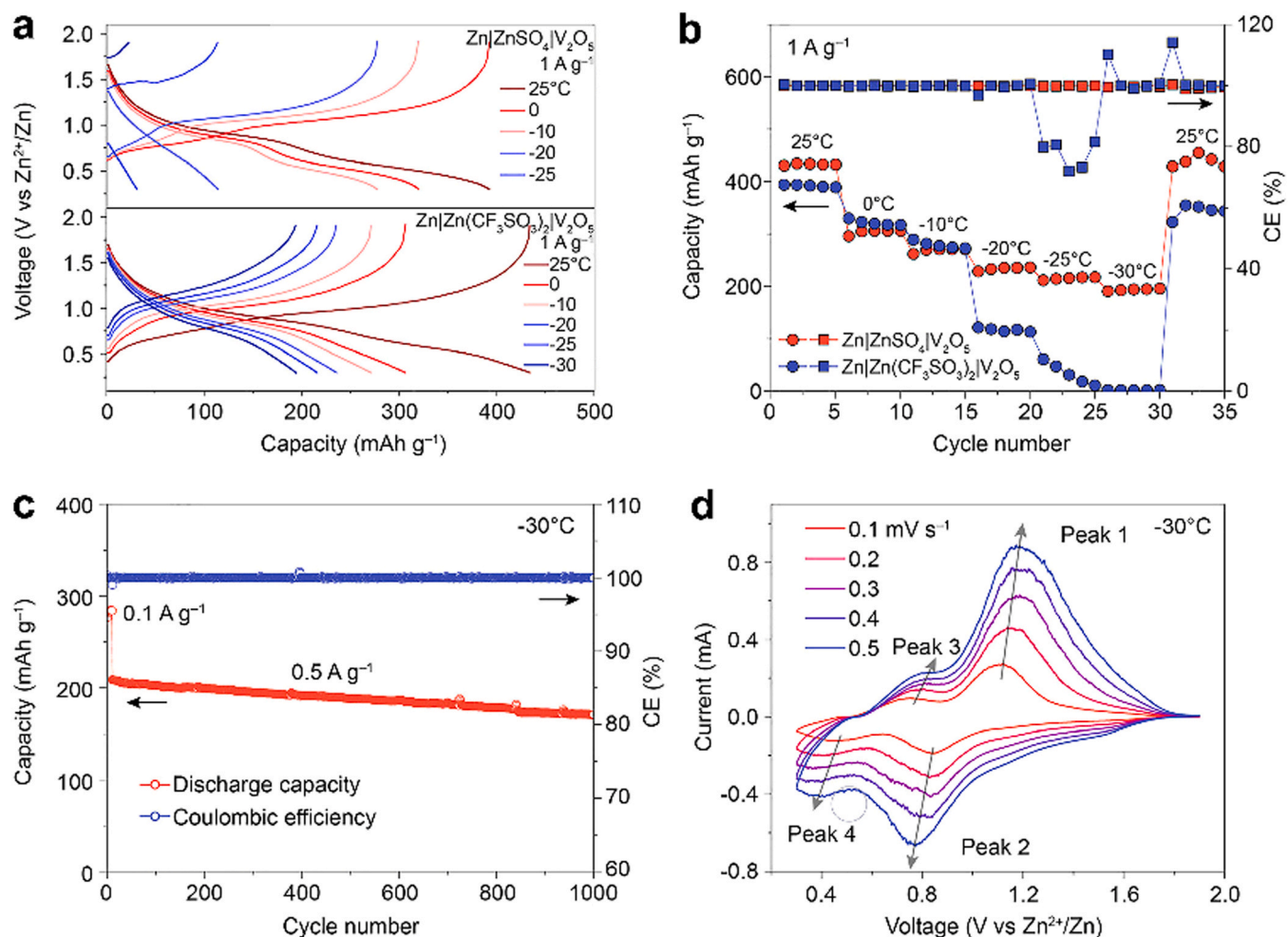


**Fig. 17.** Electrochemical performance of Zn||V<sub>2</sub>O<sub>5</sub> batteries. a Discharge-charge voltage profiles of Zn|2 M Zn||V<sub>2</sub>O<sub>5</sub> and Zn|2 M Zn(CF<sub>3</sub>SO<sub>4</sub>)<sub>2</sub>|V<sub>2</sub>O<sub>5</sub> batteries at various temperatures from 25 to -30 °C; b Discharge capacities and CEs of the two batteries from 25 to -30 °C; c Cycling performance of the Zn||V<sub>2</sub>O<sub>5</sub> battery; d CV curves of the Zn||V<sub>2</sub>O<sub>5</sub> battery.

as the cathode can provide a high specific capacity of 285.0 mAh g<sup>-1</sup> and cycle 1000 times at -30 °C after maintaining 81.7% capacity. In Fig. 17d, the CV curve shows that the electrochemical reaction is controlled by the synergistic control of ion diffusion and pseudo-capacitance.

## 5.2. Other materials

Metal hexacyanoferrates (MHCF, M=Fe, Cu, Mn, Co, Ni, etc.) are a class of metal-organic frameworks composed of linear Fe-C≡N-M [158]. Among MHCFs, cobalt hexacyanoferrate (CoHCF) is considered as a promising cathode material [159–161]. Its unique three-dimensional open framework has large-scale channels and octahedral gaps, which can ensure the rapid diffusion of alkali metal ions and sufficient energy storage space, avoiding the large volume change of alkali metal ions during the intercalation/deintercalation process. In addition, its three-dimensional framework structure endows it with high rate capability and excellent cycling stability. However, in the energy storage mechanism of CoHCF, only low-spin carbon-coordinated Fe<sup>2+</sup> can be electrochemically activated, and high-spin carbon-coordinated Co<sup>2+</sup> is inert in neutral aqueous electrolytes, which leads to its limited capacity at low temperatures [162–165].

Ma et al. [166] developed ionic liquids (ILs) that support zinc salts as electrolytes (denoted as ILZE) for zinc batteries. This electrolyte can fundamentally solve the side effects of hydrogen evolution reaction (HER) and zinc dendrite growth in zinc-ion batteries. As shown in Fig. 18a, a zinc-ion battery was constructed by using cobalt

hexacyanoferrate (CoHCF) as the cathode coupled with metallic zinc in ILZE. The CV curve results in Fig. 18b show that Fe<sup>2+</sup> and Co<sup>2+</sup> in the CoHCF lattice are fully activated in the ILZE electrolyte. The two-electron energy storage process contributed by Fe<sup>2+</sup> and Co<sup>2+</sup> enables the battery to exhibit high specific capacity. To further enable the battery to have excellent electrochemical performance at low temperatures, the researchers introduced 5% poly(ethylene oxide) (PEO) in the ILZE electrolyte. The flexibility and modulus of solid-state electrolytes can be enhanced by forming H-F bonds between PVDF-HFP and PEO molecules. Its ultra-thin and ultra-light performance reduces the areal density of solid electrolytes and increases the energy density of zinc-ion batteries. At -20 °C in Fig. 18c, its capacity retention can reach 38% of that at 25 °C.

Polyaniline (PANI), as a typical organic conducting polymer, has been widely used in different energy storage systems [167–170]. Due to its conjugated chemical bond (C=N) and long-range conjugated structure, the interaction voltage of anions with (C-N<sup>+</sup>) in oxidized PANI is often lower than that of water electrolysis, and cations can be stored in the reduced PANI (CN<sup>-</sup>) [171]. Therefore, PANI is a promising anion-cation storage guest material. However, when PANI is in a low-acid electrolyte, deprotonation will occur causing PANI to deactivate, resulting in low capacity and low rate performance.

To solve this problem and make it have excellent performance at low temperature, Lin et al. [172] developed a new hydrated deep eutectic electrolyte (DEE) using sulfolane (SL) and Zn(ClO<sub>4</sub>)<sub>2</sub>·6 H<sub>2</sub>O to prevent water-induced spoilage. Among them, water molecules form a unique water-in-DEE structure in Zn(ClO<sub>4</sub>)<sub>2</sub>·6 H<sub>2</sub>O, which helps to

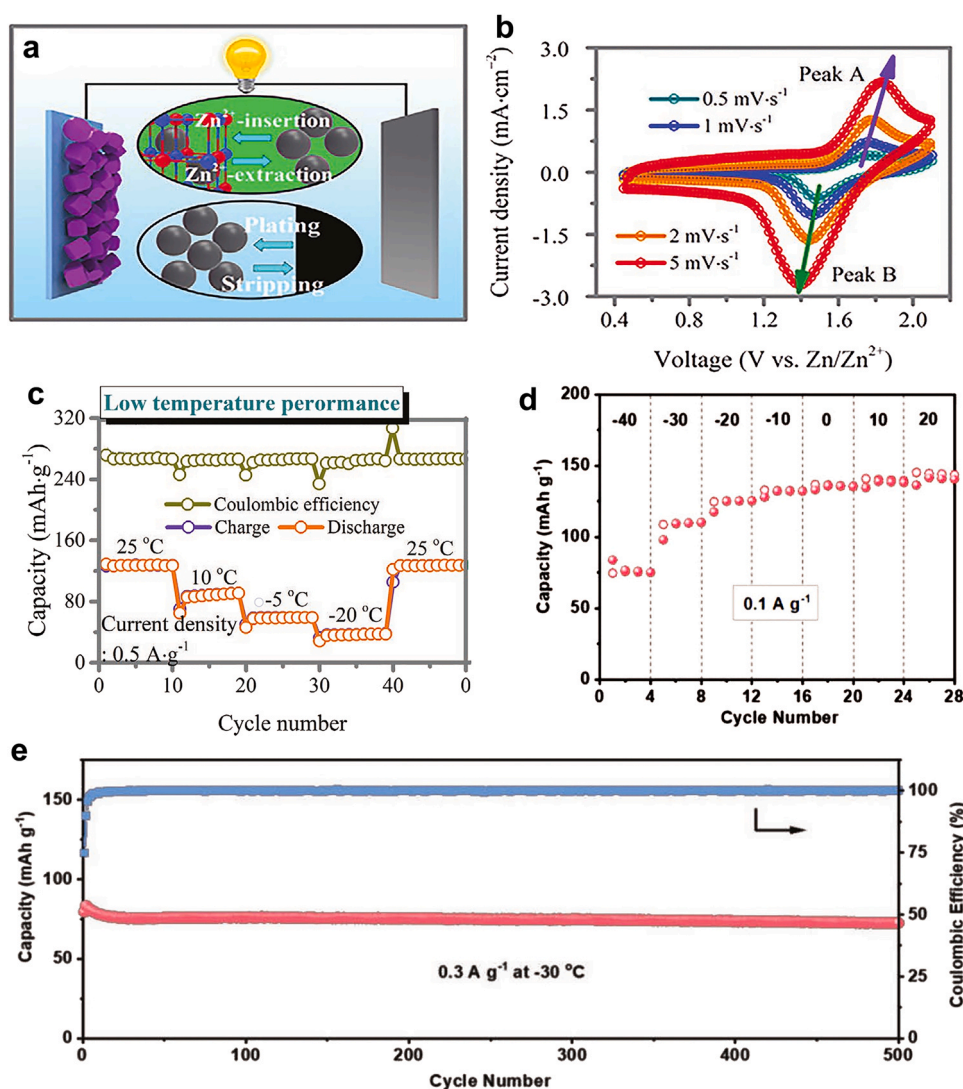


**Fig. 18.** Electrochemical performance of a Zn/CoHCF battery: a schematic illustration of Zn/CoHCF battery; b CV curves at different scan rates of 0.5, 1, 2, and 5 mV s<sup>-1</sup>; c Electrochemical performance at different temperatures from -20 to 25 °C; d Cyclic performance of the Zn=Z6S=PANI cell at 0.1 A g<sup>-1</sup> at LT (from -40 to 20 °C). e Cycling performance of 0.3 A g<sup>-1</sup> for Zn=Z6S=PANI cells at -30 °C.

improve ionic conductivity and reduce electrolyte viscosity. The strong coordination between SL and Zn<sup>2+</sup> induces a deep eutectic effect, which enables DEE to have a lower solidification temperature. In addition, DEE has a wide operating temperature. Based on the above advantages, the researchers used PANI as the cathode and selected Zn(ClO<sub>4</sub>)<sub>2</sub> · 6H<sub>2</sub>O and DEE with an SL molar ratio of 1:6 (denoted as Z6S) to fabricate a Zn=Z6S=Pani zinc-ion battery. Fig. 18d shows that the reversible capacity of this cell can reach 76 mAh g<sup>-1</sup> at 0.1 A g<sup>-1</sup> at -40 °C. Fig. 18e shows that the Zn=Z6S=Pani battery still achieves a capacity of 73 mAh g<sup>-1</sup> after 500 cycles at 0.3 A g<sup>-1</sup> at -30 °C. This shows that the battery has excellent cycling stability at low temperature under the action of DEE.

## 6. Conclusions and outlook

With the advancement of society and the development of technology, scientists are constantly exploring and developing new battery technologies that can support the next generation of power supply equipment and applications. At present, an increasing number of applications, such as electronic products, military power supplies, and space and aerospace systems, need to be used repeatedly under low temperature conditions and function normally.

In the past few decades, lithium-ion batteries have been continuously developed in these fields, but with the development of the next generation of higher energy density batteries, the low-temperature performance of sodium-ion batteries, magnesium-ion batteries, and zinc-ion batteries has gradually increased. In this review, we discussed the research status of the above four battery low-temperature cathode materials, which mainly include polyanionic cathode materials, oxide cathode materials, and Prussian blue/Prussian blue analog cathode materials. Polyanionic cathode materials provide high safety and structural stability. The voltage can be effectively increased by adding anions to its crystal lattice, the surface coating can improve conductivity, and metal ions can be doped to reduce diffusion resistance while allowing rapid insertion/desorption of ions. hence exhibiting excellent low temperature performance; the oxide cathode material can achieve high capacity and long cycle stability through interlayer doping, surface coating, and reasonable control of its structure; Prussian blue compound cathode has excellent cycle performance and rate performance, through the surface coating, rational design of the structure and other strategies to achieve excellent low temperature electrochemical performance. In addition, some batteries in addition to the design of high-energy cathode materials, but also through electrolysis Special electrolytes

or solvents are added to the liquid to ensure the battery's high-efficiency discharge performance at extremely low temperatures.

Compared with using a thermal management system to heat the battery, the low temperature battery problem can be alleviated more effectively from the perspective of battery design and battery chemistry. By coating the cathode material to improve the conductivity, doping with metal ions reduces the impedance, thereby accelerating the charge transfer and improving the low-temperature electrochemical performance. At present, the development of cathode materials for low temperature applications faces various challenges. Looking forward to the future, more attention should be paid to the ion insertion/extraction mechanism of various electrode materials at low temperatures, and extend the voltage window of cathode materials at low temperatures to obtain higher-high capacity and stable cycling performance, and design and control the self-structure of the cathode material. In addition to researching methods to improve the low-temperature performance of batteries from the cathode aspect, other strategies need to be paid attention to achieve excellent low-temperature electrochemical performance. Anode materials, electrolytes, separators, and additives are important components of batteries, and improving these parts can also ensure the high-efficiency performance of batteries at low temperatures. In addition to the lithium-ion batteries, sodium-ion batteries, magnesium-ion batteries, and zinc-ion batteries mentioned in this review, more attention should be paid to the application of other metal-ion batteries at low temperature, such as potassium-ion batteries and calcium-ion batteries.

### Declaration of Competing Interest

The authors declare that they have no known competing financial interests or personal relationships that could have appeared to influence the work reported in this paper.

### Acknowledgments

We acknowledge financial support from National Natural Science Foundation of China (Nos. 52172250, 51772296).

### References

- Z. Wang, C. Li, K. Domen, Recent developments in heterogeneous photocatalysts for solar-driven overall water splitting, *Chem. Soc. Rev.* 48 (2009) 2109–2125, <https://doi.org/10.1039/C8CS00542G>
- N. Roy, N. Suzuki, C. Terashima, A. Fujishima, Recent improvements in the production of solar fuels: from CO<sub>2</sub> reduction to water splitting and artificial photosynthesis, *Bull. Chem. Soc. Jpn.* 92 (2019) 178–192, <https://doi.org/10.1246/bcsj.20180250>
- B. Dunn, H. Kamath, J.M. Tarascon, Electrical energy storage for the grid: a battery of choices, *Science* 334 (2011) 928–935, <https://doi.org/10.1126/science.1212741>
- J.B. Goodenough, K.S. Park, The Li-ion rechargeable battery: a perspective, *J. Am. Chem. Soc.* 135 (2013) 1167–1176, <https://doi.org/10.1021/ja3091438>
- C.R. Zhu, X.H. Xia, J.L. Liu, Z.X. Fan, D.L. Chao, H. Zhang, H.J. Fan, TiO<sub>2</sub> nanotube@SnO<sub>2</sub> nanoflake core-branch arrays for lithium-ion battery anode, *Nano Energy* 4 (2014) 105–112, <https://doi.org/10.1016/j.nanoen.2013.12.018>
- A. Gupta, A. Manthiram, Designing advanced lithium-based batteries for low temperature conditions, *Adv. Energy Mater.* 10 (2020), <https://doi.org/10.1002/aenm.202001972>
- Y. Yang, P.L. Li, N. Wang, Z. Fang, C.X. Wang, X.L. Dong, Y.Y. Xia, Fluorinated carboxylate ester-based electrolyte for lithium ion batteries operated at low temperature, *Chem. Commun.* 56 (2022) 9640–9643, <https://doi.org/10.1039/D0CC04049E>
- X.L. Dong, Y. Yang, B.L. Wang, Y.J. Cao, N. Wang, P.L. Li, Y.G. Wang, Y.Y. Xia, Low-temperature charge/discharge of rechargeable battery realized by intercalation pseudocapacitive behavior, *Adv. Sci.* 7 (2020), <https://doi.org/10.1002/advs.202000196>
- C.Y. Wang, G.S. Zhang, S.H. Ge, T. Xu, Y. Ji, X.G. Yang, Y.J. Leng, Lithium-ion battery structure that self-heats at low temperatures, *Nature* 529 (2016) 515–518, <https://doi.org/10.1038/nature16502>
- J.B. Hou, M. Yang, D.Y. Wang, J.L. Zhang, Fundamentals and challenges of lithium ion batteries at temperatures between –40 and 60°C, *Adv. Energy Mater.* 10 (2020), <https://doi.org/10.1002/aenm.201904152>

- G.L. Zhu, K.C. Wen, W.Q. Lv, X.Z. Zhou, Y.C. Liang, F. Yang, Z.L. Chen, M.Z.J.C. Li, Y.Q. Zhang, W.D. He, Materials insights into low temperature performances of lithium-ion batteries, *J. Power Sources* 300 (2015) 29–40, <https://doi.org/10.1016/j.jpowsour.2015.09.056>
- X.L. Dong, Z.W. Guo, Z.Y. Guo, Y.G. Wang, Y.Y. Xia, Organic batteries operated at –70°C, *Joule* 2 (2018) 902–913, <https://doi.org/10.1016/j.joule.2018.01.017>
- W.Y. Chang, S.J. Kim, I.T. Park, B.W. Cho, K.F. Chung, H.C. Shin, Low temperature performance of LiFePO<sub>4</sub> cathode material for Li-ion batteries, *J. Alloy. Compd.* (2013), <https://doi.org/10.1016/j.jallcom.2013.02.143>
- X.L. Wu, Y.G. Guo, J. Su, J.W. Xiong, Y.L. Zhang, L.J. Wan, Carbon-nanotube-decorated nano-LiFePO<sub>4</sub>@C cathode material with superior high-rate and low-temperature performances for lithium-ion batteries, *Adv. Energy Mater.* 3 (2013) 1155–1160, <https://doi.org/10.1002/aenm.201300159>
- T.R. Jow, S.A. Delp, J.L. Allen, J.P. Jones, M.C. Smart, Factors limiting Li<sup>+</sup> charge transfer kinetics in Li-ion batteries, *J. Electrochem. Soc.* 165 (2018), <https://doi.org/10.1149/2.1221802jes>
- S. Ma, M. Jiang, P. Tao, C.Y. Song, J.B. Wu, J. Wang, Temperature effect and thermal impact in lithium-ion batteries: a review, *Prog. Nat. Sci. Mater.* 28 (2018) 653–666, <https://doi.org/10.1016/j.pnsc.2018.11.002>
- G.D. Fan, K. Pan, M. Canova, J. Marcicki, X.G. Yang, Modeling of Li-ion cells for fast simulation of high C-rate and low temperature operations, *J. Electrochem. Soc.* 163 (2016), <https://doi.org/10.1149/1945-7111/abc4bc>
- H.M. Cho, W.S. Choi, J.Y. Go, S.E. Bae, H.C. Shin, A study on time-dependent low temperature power performance of a lithium-ion battery, *J. Power Sources* 198 (2012) 273–280, <https://doi.org/10.1016/j.jpowsour.2011.09.111>
- N. Yabuuchi, K. Kubota, M. Dahbi, S. Komaba, Research development on sodium-ion batteries, *Chem. Rev.* 114 (2014) 11636–11682, <https://doi.org/10.1021/cr500192f>
- J. Xie, Q.C. Zhang, Recent progress in multivalent metal (Mg, Zn, Ca, and Al) and metal-ion rechargeable batteries with organic materials as promising electrodes, *Small* 15 (2019), <https://doi.org/10.1002/sml.201805061>
- J. Emsley, *Nature's Building Blocks: An AZ Guide to the Elements*, Oxford University Press, 2011.
- Y. Orikasa, T. Masese, Y. Koyama, T. Mori, M. Hattori, K. Yamamoto, T. Okado, Z.D. Huang, T. Minato, C. Tassel, J. Kim, Y. Kobayashi, T. Abe, H. Kageyama, Y. Uchimoto, High energy density rechargeable magnesium battery using earth-abundant and non-toxic elements, *Sci. Rep.* 4 (2014) 1–6, <https://doi.org/10.1038/srep05622>
- X.H. Rui, X.H. Zhang, S.T. Xu, H.T. Tan, Y. Jiang, L.Y. Gan, Y.Z. Feng, C.C. Li, A low-temperature sodium-ion full battery: superb kinetics and cycling stability, *Adv. Funct. Mater.* 31 (2021), <https://doi.org/10.1002/adfm.202009458>
- K.J. Zhu, Z.P. Li, Z.Q. Sun, P. Liu, T. Jin, X.C. Chen, H.X. Li, W.B. Lu, L.F. Jiao, Inorganic electrolyte for low-temperature aqueous sodium ion batteries, *Small* (2022), <https://doi.org/10.1002/sml.202107662>
- X.H. Rui, X.H. Zhang, S.T. Xu, H.T. Tan, Y. Jiang, L.Y. Gan, Y.Z. Feng, C.C. Li, Y. Yu, A low-temperature sodium-ion full battery: superb kinetics and cycling stability, *Adv. Funct. Mater.* 31 (2021), <https://doi.org/10.1002/adfm.202009458>
- J.Y. Liu, Y. Zhong, X.L. Li, T.X. Ying, T.L. Han, J.J. Lin, A novel rose-with-thorn ternary MoS<sub>2</sub>@carbon@polyaniline nanocomposite as a rechargeable magnesium battery cathode displaying stable capacity and low-temperature performance, *Nanoscale Adv.* 3 (2021) 5576–5580, <https://doi.org/10.1039/D1NA00445J>
- T.J. Sun, X.M. Yuan, K. Wang, S.B. Zheng, J.Q. Shi, Q. Zhang, W.S. Cai, J. Liang, Z.L. Tao, An ultralow-temperature aqueous zinc-ion battery, *J. Mater. Chem. A* 9 (2021) 7042–7047, <https://doi.org/10.1039/D0TA12409E>
- S.F. Chen, Y.F. Zhang, H.B. Geng, Y. Yang, X.H. Rui, C.C. Li, Zinc ions pillared vanadate cathodes by chemical pre-intercalation towards long cycling life and low-temperature zinc ion batteries, *J. Power Sources* 441 (2019), <https://doi.org/10.1016/j.jpowsour.2019.227192>
- Y. Ji, C.Y. Wang, Heating strategies for Li-ion batteries operated from subzero temperatures, *Electrochem. Acta* 107 (2013) 664–674, <https://doi.org/10.1016/j.electacta.2013.03.147>
- W.F. Li, H.W. Wang, Y.J. Zhang, M.G. Ouyang, Flammability characteristics of the battery vent gas: a case of NCA and LFP lithium-ion batteries during external heating abuse, *J. Energy Storage* 24 (2019), <https://doi.org/10.1016/j.est.2019.100775>
- S.S. Guo, R. Xiong, K. Wang, F.C. Sun, A novel echelon internal heating strategy of cold batteries for all-climate electric vehicles application, *Appl. Energy* 219 (2018) 256–263, <https://doi.org/10.1016/j.apenergy.2018.03.052>
- J.C. Jiang, H.J. Ruan, B.X. Sun, L.Y. Wang, W.Z. Gao, W.G. Zhang, A low-temperature internal heating strategy without lifetime reduction for large-size automotive lithium-ion battery pack, *Appl. Energy* 230 (2018) 257–266, <https://doi.org/10.1016/j.apenergy.2018.08.070>
- M.C. Smart, B.V. Ratnakumar, K.B. Chin, L.D. Whitcanack, Lithium-ion electrolytes containing ester cosolvents for improved low temperature performance, *J. Electrochem. Soc.* 157 (2010).
- S. Tan, U.N.D. Rodrigo, Z. Shadike, B. Lucht, K. Xu, C.S. Wang, X.Q. Yang, E.Y. Hu, Novel low-temperature electrolyte using isoxazole as the main solvent for lithium-ion batteries, *ACS Appl. Mater. Interfaces* 13 (2021) 24995–25001, <https://doi.org/10.1021/acsami.1c05894>
- J. Qin, Q. Lan, N. Liu, Y.L. Zhao, Z.P. Song, H. Zhan, A metal-free battery working at –80°C, *Energy Storage Mater.* 26 (2020) 585–592, <https://doi.org/10.1016/j.ensm.2019.12.002>
- J. Holoubek, H.D. Liu, Z.H. Wu, Y.J.Y.X. Xing, G.R. Cai, S.C.Y.H.Y. Zhao, T.A. Pascal, Z. Chen, P. Liu, Tailoring electrolyte solvation for li metal batteries cycled at

- ultra-low temperature, *Nat. Energy* 6 (2021) 303–313, <https://doi.org/10.1038/s41560-021-00783-z>
- [37] J. Holoubek, Y. Yin, M.Q. Li, M.Y. Yu, Y.S. Meng, P. Liu, Z. Chen, Exploiting mechanistic solvation kinetics for dual-graphite batteries with high power output at extremely low temperature, *Angew. Chem. Int. Ed.* 131 (2019) 19068–19073, <https://doi.org/10.1002/ange.201912167>
- [38] X.L. Fan, X. Ji, L. Chen, J. Chen, T. Deng, F.D. Han, J. Yue, N. Piao, R.X. Wang, X.Q. Zhou, X.Z. Xiao, L.X. Chen, C.S. Wang, All-temperature batteries enabled by fluorinated electrolytes with non-polar solvents, *Nat. Energy* 4 (2019) 882–890, <https://doi.org/10.1038/s41560-019-0474-3>
- [39] B. Liao, H.Y. Li, M.Q. Xu, L.D. Xing, Y.H. Liao, X.B. Ren, W.Z. Fan, L. Yu, K. Xu, W.S. Li, Designing low impedance interface films simultaneously on anode and cathode for high energy batteries, *Adv. Energy Mater.* 8 (2018), <https://doi.org/10.1002/aenm.201800802>
- [40] X.L. Dong, Y. Yang, B.L. Wang, Y.J. Cao, N. Wang, P.L. Li, Y.G. Wang, Y.Y. Xia, Low-temperature charge/discharge of rechargeable battery realized by intercalation pseudocapacitive behavior, *Adv. Sci.* 7 (2020), <https://doi.org/10.1002/adv.202000196>
- [41] J. Xu, X. Wang, N.Y. Yuan, B.Q. Hu, J.N. Ding, Graphite-based lithium ion battery with ultrafast charging and discharging and excellent low temperature performance, *J. Power Sources* 430 (2019) 74–79, <https://doi.org/10.1016/j.jpowsour.2019.05.024>
- [42] X.L. Dong, Y. Yang, P.L. Li, Z. Fang, Y.G. Wang, Y.Y. Xia, A high-rate and long-life rechargeable battery operated at  $-75^{\circ}\text{C}$ , *Batteries Supercaps* 3 (2020) 1016–1020, <https://doi.org/10.1002/batt.202000117>
- [43] B.Q. Liu, Q. Zhang, L. Li, L.Y. Zhang, Z.S. Jin, C.G. Wang, Z.M. Su, Achieving highly electrochemically active maricite  $\text{NaFePO}_4$  with ultrafine  $\text{NaFePO}_4$ @C subunits for high rate and low temperature sodium-ion batteries, *Chem. Eng. J.* 405 (2021), <https://doi.org/10.1016/j.cej.2020.126689>
- [44] Mn-doped  $\text{Na}_4\text{Fe}_3(\text{PO}_4)_2(\text{P}_2\text{O}_7)$  facilitating  $\text{Na}^+$  migration at low temperature as a high performance cathode material of sodium ion batteries, *J. Power Sources*, 521, 2022, (<https://doi.org/10.1016/j.jpowsour.2021.230922>).
- [45] L.B. Ran, A. Baktash, M. Li, Y. Yin, B. Demir, T. Lin, M. Li, M. Rana, L. gentle, L.Z. Wang, D.J. Searles, R. Knibbe, S. Ge co-doping NASICON boosts solid-state sodium ion batteries' performance, *Energy Storage Mater.* 40 (2021) 282–291, <https://doi.org/10.1016/j.ensm.2021.05.017>
- [46] Trigger  $\text{Na}^+$ -solvent co-intercalation to achieve high-performance sodium-ion batteries at subzero temperature, *Chem. Eng. J.*, 430, 2022, (<https://doi.org/10.1016/j.cej.2021.132750>).
- [47] X.W. Wang, W.M.Z. Zhang W., K.W. Wong, J.W. Wu, T. Chen, S.M. Huang, Ultrafine ZnSe encapsulated in nitrogen-doped porous carbon nanofibers for superior Na-ion batteries with a long lifespan and low-temperature performance, *ACS Sustain. Chem. Eng.* 9 (2021) 11705–11713, <https://doi.org/10.1021/acssuschemeng.1c02447>
- [48] C.Y. Pei, Y.M. Yin, R.M. Sun, F.Y. Xiong, X.B. Liao, H. Tang, S.S. Tan, Y. Zhao, Q.Y. An, L.Q. Mai, Interchain-expanded vanadium tetrasulfide with fast kinetics for rechargeable magnesium batteries, *ACS Appl. Mater. Interfaces* 11 (2019) 31954–31961, <https://doi.org/10.1021/acsami.9b09592>
- [49] D. Lu, H.Q. Liu, T. Huang, Z.X. Xu, L. Ma, P. Yang, P.R. Qiang, F. Zhang, D.Q. Wu, Magnesium ions based organic secondary battery, *J. Mater. Chem. A* 6 (2018) 17297–17302, <https://doi.org/10.1039/C8TA05230A>
- [50] T.J. Sun, S.B. Zheng, H.H. Du, Z.L. Tao, Synergistic effect of cation and anion for low-temperature aqueous zinc-ion battery, *Nano-Micro Lett.* 13 (2021) 1–10, <https://doi.org/10.1007/s40820-021-00733-0>
- [51] W.W. Xu, C.Z. Liu, S.X. Ren, D. Lee, J. Gwon, J.C. Flake, T.Z. Lei, N. Baisakh, Q.L. Wu, A cellulose nanofiber–polyacrylamide hydrogel based on a co-electrolyte system for solid-state zinc ion batteries to operate at extremely cold temperatures, *J. Mater. Chem. A* 9 (2021) 25651–25662, <https://doi.org/10.1039/D1TA08023G>
- [52] C.F. Lin, F.Q. Qi, H.L. Dong, X. Li, C.P. Shen, E.H. Ang, Y.Q. Han, H.B. Geng, C.C. Li, Suppressing vanadium dissolution of  $\text{V}_2\text{O}_5$  via in situ polyethylene glycol intercalation towards ultralong lifetime room/low-temperature zinc-ion batteries, *Nanoscale* 13 (2021) 17040–17048, <https://doi.org/10.1039/D1NR05334E>
- [53] J. Xu, X. Wang, N.Y. Yuan, J.N. Ding, S. Qin, J.M. Razal, X.H. Wang, S.H. Ge, Y. Gogotsi, Extending the low temperature operational limit of Li-ion battery to  $-80^{\circ}\text{C}$ , *Energy Storage Mater.* 23 (2019) 383–389, <https://doi.org/10.1016/j.ensm.2019.04.033>
- [54] N. Chang, T.Y. Li, R. Li, S.N. Wang, Y.B. Yin, H.M. Zhang, X.F. Li, An aqueous hybrid electrolyte for low temperature zinc-based energy storage devices, *Energy Environ. Sci.* 13 (2020) 3527–3535, <https://doi.org/10.1039/D0EE01538E>
- [55] J.X. Li, L. Wang, Y. Zhao, S.Y. Li, X.M. FU, B.J. Wang, H.S. Peng, Li- $\text{CO}_2$  batteries efficiently working at ultra-low temperatures, *Adv. Funct. Mater.* 30 (2020), <https://doi.org/10.1002/adfm.202001619>
- [56] Q.Q. Xiong, J.J. Lou, X.J. Teng, X.X. Lu, H.Z. Chi, Z.G. Ji, Controllable synthesis of  $\text{NC@LiFePO}_4$  nanospheres as advanced cathode of lithium-ion batteries, *J. Alloy. Compd.* 743 (2018) 377–382, <https://doi.org/10.1016/j.jallcom.2018.01.350>
- [57] Y.J. Fang, J.X. Zhang, L.F. Xiao, X.P. Ai, Y.L. Cao, H.X. Yang, Phosphate framework electrode materials for sodium ion batteries, *Adv. Sci.* 4 (2017), <https://doi.org/10.1002/adv.201600392>
- [58] Y.G. Wang, P. He, H.S. Zhou, Olivine  $\text{LiFePO}_4$ : development and future, *Energy Environ. Sci.* 4 (2011) 805–817, <https://doi.org/10.1039/C0EE00176G>
- [59] B.L. Ellis, K.T. Lee, L.F. Nazar, Positive electrode materials for Li-ion and Li-batteries, *Chem. Mater.* 22 (2010) 691–714, <https://doi.org/10.1021/cm902696j>
- [60] K. Zaghib, A. Guerfi, P. Hovington, A. Vijh, M. Trudeau, A. Mauger, J.B. Goodenough, C.M. Julien, Review and analysis of nanostructured olivine-based lithium rechargeable batteries: Status and trends, *J. Power Sources* 232 (2013) 357–369, <https://doi.org/10.1016/j.jpowsour.2012.12.095>
- [61] P.P. Prossini, M. Lisi, D. Zane, M. Pasquali, Determination of the chemical diffusion coefficient of lithium in  $\text{LiFePO}_4$ , *Solid State Ion.* 148 (2002) 45–51, [https://doi.org/10.1016/S0167-2738\(02\)00134-0](https://doi.org/10.1016/S0167-2738(02)00134-0)
- [62] L.X. Yuan, Z.H. Wang, W.X. Zhang, X.L. Hu, J.T. Chen, Y.H. Huang, J.B. Goodenough, Development and challenges of  $\text{LiFePO}_4$  cathode material for lithium-ion batteries, *Energy Environ. Sci.* 4 (2011) 269–284, <https://doi.org/10.1039/C0EE00029A>
- [63] Y.N. Xu, S.Y. Chung, J.T. Bloking, Y.M. Chiang, W.Y. Ching, Electronic structure and electrical conductivity of undoped  $\text{LiFePO}_4$ , *Electrochem. Solid. State Lett.* 7 (2004), <https://doi.org/10.1149/1.1703470>
- [64] P.P. Prossini, M. Lisi, D. Zane, M. Pasquali, Determination of the chemical diffusion coefficient of lithium in  $\text{LiFePO}_4$ , *Solid State Ion.* 148 (2002) 45–51, [https://doi.org/10.1016/S0167-2738\(02\)00134-0](https://doi.org/10.1016/S0167-2738(02)00134-0)
- [65] R. Amin, J. Maier, P. Balaya, D.P. Chen, C.T. Lin, Ionic and electronic transport in single crystalline  $\text{LiFePO}_4$  grown by optical floating zone technique, *Solid State Ion.* 179 (2008) 1683–1687, <https://doi.org/10.1016/j.ssi.2008.01.079>
- [66] J.Y. Li, W.L. Yao, S. Martin, D. Vaknin, Lithium ion conductivity in single crystal  $\text{LiFePO}_4$ , *Solid State Ion.* 179 (2008) 2016–2019, <https://doi.org/10.1016/j.ssi.2008.06.028>
- [67] D. Lepage, F. Sobh, C. Kuss, G. Liang, S.B. Schougaard, Delithiation kinetics study of carbon coated and carbon free  $\text{LiFePO}_4$ , *J. Power Sources* 256 (2014) 61–65, <https://doi.org/10.1016/j.jpowsour.2013.12.054>
- [68] S.W. Oh, S.T. Myung, S.M. Oh, K.H. Oh, K. Amine, B. Scrosati, Y.K. Sun, Double carbon coating of  $\text{LiFePO}_4$  as high rate electrode for rechargeable lithium batteries, *Adv. Mater.* 22 (2010) 4842–4845, <https://doi.org/10.1002/adma.200904027>
- [69] Y. Zhang, G.J. Shao, Z.P. Ma, G.L. Wang, J.P. Du, Influence of surface modification by vanadium oxide and carbon on the electrochemical performance of  $\text{LiFePO}_4/\text{C}$ , *Ionics*, 19(8), pp. 1091–1097, (<https://doi.org/10.1007/s11581-012-0828-3>).
- [70] J. Song, W.B. Wang, C.E. Carr, Z.D. Dai, Y.Z. Tang, Vestibular nuclei characterized by calcium-binding protein immunoreactivity and tract tracing in Gekko gekko, *Hear. Res.* 296 (2013) 1–12, <https://doi.org/10.1016/j.heares.2012.11.011>
- [71] Y.Q. Wang, Z.P. Liu, S.M. Zhou, An effective method for preparing uniform carbon coated nanosized  $\text{LiFePO}_4$  particles, *Electrochim. Acta* 58 (2011) 359–363, <https://doi.org/10.1016/j.electacta.2011.09.053>
- [72] A. Kuwahara, S. Suzuki, M. Miyayama, Hydrothermal synthesis of  $\text{LiFePO}_4$  with small particle size and its electrochemical properties, *J. Electroceram.* 24 (2010) 69–75, <https://doi.org/10.1007/s10832-008-9442-1>
- [73] Z.H. Chen, Y. Qin, K. Amine, Y.K. Sun, Role of surface coating on cathode materials for lithium-ion batteries, *J. Mater. Chem. C* 20 (2010) 7606–7612, <https://doi.org/10.1039/C0JM00154F>
- [74] P.Y. Guan, L. Zhou, Z.L. Yu, Y.D. Sun, Y.J. Liu, F.X. Wu, Y.F. Jiang, D.W. Chu, Recent progress of surface coating on cathode materials for high-performance lithium-ion batteries, *J. Energy Chem.* 43 (2020) 220–235, <https://doi.org/10.1016/j.jechem.2019.08.022>
- [75] Q.B. Liu, S.J. Liao, H.Y. Song, Z.X. Liang, High-performance  $\text{LiFePO}_4/\text{C}$  materials: effect of carbon source on microstructure and performance, *J. Power Sources* 211 (2012) 52058, <https://doi.org/10.1016/j.jpowsour.2012.03.090>
- [76] Y. Kadoma, J.M. Kim, K. Abiko, K. Ohtsuki, K. Ui, N. Kumagai, Optimization of electrochemical properties of  $\text{LiFePO}_4/\text{C}$  prepared by an aqueous solution method using sucrose, *Electrochim. Acta* 55 (2010) 1034–1041, <https://doi.org/10.1016/j.electacta.2009.09.029>
- [77] B. Yao, Z.J. Ding, J.X. Zhang, X.Y. Feng, L.W. Yin, Encapsulation of  $\text{LiFePO}_4$  by insitu graphitized carbon cage towards enhanced low temperature performance as cathode materials for lithium-ion batteries, *J. Solid State Chem.* 216 (2014) 9–12, <https://doi.org/10.1016/j.jssc.2014.04.023>
- [78] Y.B. Lin, Y. Lin, T. Zhou, G.Y. Zhao, Y.D. Huang, Z.G. Huang, Enhanced electrochemical performances of  $\text{LiFePO}_4/\text{C}$  by surface modification with Sn nanoparticles, *J. Power Sources* 226 (2013) 20–26, <https://doi.org/10.1016/j.jpowsour.2012.10.074>
- [79] G.L. Lan, R.S. Guo, L. Liu, Y.X. Yang, C. Zhang, C. Wu, W.N. Guo, H. Jiang, Enhanced low temperature electrochemical performances of  $\text{LiFePO}_4/\text{C}$  by surface modification with  $\text{Ti}_3\text{SiC}_2$ , *J. Power Sources* 288 (2015) 136–144, <https://doi.org/10.1016/j.jpowsour.2015.04.129>
- [80] X.L. Cui, K.Y. Tuo, Y.C. Xie, C.L. Liu, D.N. Zhao, L. Yang, X.L. Fu, S.Y. Li, Investigation on electrochemical performance at the low temperature of LFP/CP composite based on phosphorus doped carbon network, *Ionics* 26 (2020) 3795–3808, <https://doi.org/10.1007/s11581-020-03567-9>
- [81] C.L. Li, Y.C. Xie, N.S. Zhang, L. Ai, Y.W. Liang, K.Y. Tuo, X.S. Ye, G.F. Jia, S.Y. Li, Optimization of  $\text{LiFePO}_4$  cathode material based on phosphorus doped graphite network structure for lithium ion batteries, *Ionics* 25 (2019) 927–937, <https://doi.org/10.1007/s11581-018-2744-7>
- [82] B. Yao, Z.J. Ding, J.X. Zhang, X.Y. Feng, L.W. Yin, Encapsulation of  $\text{LiFePO}_4$  by insitu graphitized carbon cage towards enhanced low temperature performance as cathode materials for lithium ion batteries, *J. Solid State Chem.* 216 (2014) 9–12, <https://doi.org/10.1016/j.jssc.2014.04.023>
- [83] C.R. Sides, C.R. Martin, Nanostructured electrodes and the low-temperature performance of Li-ion batteries, *Adv. Mater.* 17 (2005) 125–128, <https://doi.org/10.1002/adma.200400517>
- [84] B.K. Zou, H.Y. Wang, Z.Y. Qiang, Y. Shao, X. Sun, Z.Y. Wen, C.H. Chen, Mixed-carbon-coated  $\text{LiMn}_{0.4}\text{Fe}_{0.6}\text{PO}_4$  nanopowders with excellent high rate and low temperature performances for lithium-ion batteries, *Electrochim. Acta* 196 (2016) 377–385, <https://doi.org/10.1016/j.electacta.2016.03.017>

- [85] B. Eills, H.P. Subramanya, Y.H. Rho, Nanostructured materials for lithium-ion batteries: surface conductivity vs. bulk ion/electron transport, *Faraday Discuss.* 134 (2007) 415–419, 119–141, 215–233.
- [86] N.N. Zhao, Y.S. Li, X.X. Zhao, X.K. Zhi, G.C. Liang, Effect of particle size and purity on the low temperature electrochemical performance of LiFePO<sub>4</sub>/C cathode material, *J. Alloy. Compd.* 683 (2016) 123–132, <https://doi.org/10.1016/j.jallcom.2016.04.070>
- [87] P.G. Bruce, B. Scrosati, J.M. Tarascon, Nanomaterials for rechargeable lithium batteries, *Angew. Chem. Int. Ed.* 47 (2008) 2930–2946, <https://doi.org/10.1002/anie.200702505>
- [88] K. Kubota, S. Kumakura, Y. Yoda, K. Kuroki, S. Komaba, Electrochemistry and solid-state chemistry of NaMeO<sub>2</sub> (Me = 3d transition metals), *Adv. Energy Mater.* 8 (2018), <https://doi.org/10.1002/aenm.201703415>
- [89] P.P. Wang, C.Y. Xu, W.D. Li, L. Wang, L. Zhen, Low temperature electrochemical performance of β-LixV<sub>2</sub>O<sub>5</sub> cathode for lithium-ion batteries, *Electrochem. Acta* 169 (2015) 440–446, <https://doi.org/10.1016/j.electacta.2015.04.084>
- [90] C. Leger, Structural and electrochemical properties of ω-LixV<sub>2</sub>O<sub>5</sub> (0.4 < x < 3) as rechargeable cathodic material for lithium batteries, *J. Electrochem. Soc.* 152 (2005), <https://doi.org/10.1149/1.1836155>
- [91] J. Galy, J. Darriet, A. Casalat, J.B. Goodenough, J.B. Goodenough, Structure of the M<sub>x</sub>V<sub>2</sub>O<sub>5</sub>-β and M<sub>x</sub>V<sub>2</sub>-<sub>y</sub>T<sub>2</sub>O<sub>5</sub>-β phases, *Solid State Chem.* 1 (1970) 339–348, [https://doi.org/10.1016/0022-4596\(70\)90114-3](https://doi.org/10.1016/0022-4596(70)90114-3)
- [92] H.M. Liu, Y.G. Wang, L. Li, K.X. Wang, E. Hosono, H.S. Zhou, Facile synthesis of NaV<sub>6</sub>O<sub>15</sub> nanorods and its electrochemical behavior as cathode material in rechargeable lithium batteries, *J. Mater. Chem.* 19 (2009) 7885–7891, <https://doi.org/10.1039/B912906E>
- [93] P.P. Wang, C.Y. Xu, W.D. Li, L. Wang, L. Zhen, Low temperature electrochemical performance of β-LixV<sub>2</sub>O<sub>5</sub> cathode for lithium-ion batteries, *Electrochem. Acta* 169 (2015) 440–446, <https://doi.org/10.1016/j.electacta.2015.04.084>
- [94] V. Augustyn, P. Simon, B. Dunn, Pseudocapacitive oxide materials for high-rate electrochemical energy storage, *Energy Environ. Sci.* 7 (2014) 1597–1614, <https://doi.org/10.1039/C3EE44164D>
- [95] Y.Q. Jiang, J.P. Liu, Definitions of pseudocapacitive materials: a brief review, *Energy Environ. Mater.* 2 (2019) 30–37, <https://doi.org/10.1002/eem2.12028>
- [96] V. Augustyn, J. Come, M.A. Lowe, J.W. Kim, P.L. Taberna, S.H. Tolbert, H.D. Abruna, P. Simon, B. Dunn, High-rate electrochemical energy storage through Li<sup>+</sup> intercalation pseudocapacitance, *Nat. Mater.* 12 (2013) 518–522, <https://doi.org/10.1038/nmat3601>
- [97] X.L. Dong, Y. Yang, P.L. Li, Z. Fang, Y.G. Wang, Y.Y. Xia, A high-rate and long-life rechargeable battery operated at -75°C, *Batteries Supercaps* 3 (2020) 1016–1020, <https://doi.org/10.1002/batt.202000117>
- [98] J.W. Fergus, Recent developments in cathode materials for lithium ion batteries, *J. Power Sources* 195 (2010) 939–954, <https://doi.org/10.1016/j.jpowsour.2009.08.089>
- [99] C.K. Chan, H.L. Peng, G. Liu, K. McIlwrath, X.F. Zhang, R.A. Huggins, Y. Cui, High-performance lithium battery anodes using silicon nanowires, *Nat. Nanotechnol.* 3 (2008) 31–35, <https://doi.org/10.1038/nnano.2007.411>
- [100] C. Delacourt, P. Poizat, S. Levasseur, C. Masquelier, Size effects on carbon-free LiFePO<sub>4</sub> powders: the key to superior energy density, *Electrochem. Solid State Lett.* 9 (2006), <https://doi.org/10.1149/1.2201987>
- [101] B. Kang, G. Ceder, Battery materials for ultrafast charging and discharging, *Nature* 458 (2009) 190–193, <https://doi.org/10.1038/nature07853>
- [102] K.S. Chen, R. Xu, N.S. Luu, E.B. Secor, K. Hamamoto, Q.Q. Li, S. Kim, V.K. Sangwan, I. Balla, L.M. Guiney, J.W.T. Seo, X.K. Yu, W.W. Liu, J.S. Wu, C. Wolverton, V.P. Dravid, S.A. Barntt, J. Lu, K. Amine, M.C. Hersam, Comprehensive enhancement of nanostructured lithium-ion battery cathode materials via conformal graphene dispersion, *Nano Lett.* 17 (2017) 2539–2546, <https://doi.org/10.1021/acs.nanolett.7b00274>
- [103] N. Yabuuchi, K. Kubota, M. Dahbi, S. Komaba, Research development on sodium-ion batteries, *Chem. Rev.* 114 (2014) 11636–11682, <https://doi.org/10.1021/cr500192f>
- [104] M.L. Orcid, J. Hong, J. Lopez, Y.M. Sun, D.W. Feng, K. Lim, W.C. Chueh, M.F. Toney, Y. Cui, Z. Bao, High-performance sodium-organic battery by realizing four-sodium storage in disodium rhodizonate, *Nat. Energy* 2 (2017) 861–868, <https://doi.org/10.1038/s41560-017-0014-y>
- [105] W.D. Zhou, H.C. Gao, J.B. Goodenough, Low-cost hollow mesoporous polymer spheres and all-solid-state lithium, sodium batteries, *Adv. Energy Mater.* 6 (2016), <https://doi.org/10.1002/aenm.201501802>
- [106] L. Wang, Y.H. Lu, J. Liu, M.W. Xu, J.G. Cheng, D.W. Zhang, J.B. Goodenough, A superior low-cost cathode for a Na-ion battery, *Angew. Chem.* 125 (2013) 2018–2021, <https://doi.org/10.1002/ange.201206854>
- [107] J. Song, L. Wang, Y.H. Lu, J. Liu, B.K. Guo, P.H. Xiao, J.J. Lee, X.Q. Yang, G. Henkelman, J.B. Goodenough, Removal of interstitial H<sub>2</sub>O in hexacyanometallates for a superior cathode of a sodium-ion battery, *J. Am. Chem. Soc.* 137 (2015) 2658–2664, <https://doi.org/10.1021/ja512383b>
- [108] Y. You, X.L. Wu, Y.X. Yin, Y.G. Guo, High-quality Prussian blue crystals as superior cathode materials for room-temperature sodium-ion batteries, *Energy Environ. Sci.* 7 (2014) 1643–1647, <https://doi.org/10.1039/C3EE44004D>
- [109] A. Rudola, D. Kang, P. Balaya, Monoclinic sodium iron hexacyanoferrate cathode and nonflammable glyme-based electrolyte for inexpensive sodium-ion batteries, *J. Electrochem. Soc.* 164 (2017), <https://doi.org/10.1149/2.0701706jes>
- [110] J.P. Wu, J. Song, K.H. Dai, Z.Q. Zhou, L.A. Wray, G. Liu, Z.X. Shen, R. Zeng, Y.H. Lu, W.L. Yang, Modification of transition-metal redox by interstitial water in hexacyanometalate electrodes for sodium-ion batteries, *J. Am. Chem. Soc.* 139 (2017) 18358–18364, <https://doi.org/10.1021/jacs.7b10460>
- [111] G.Y. Du, M.L. Tao, J. Li, T.T. Yang, W. Gao, J.H. Deng, Y. Qi, S.J. Bao, M.W. Xu, Low-operating temperature, high-rate and durable solid-state sodium-ion battery based on polymer electrolyte and prussian blue cathode, *Adv. Energy Mater.* 10 (2020), <https://doi.org/10.1002/aenm.20190351>
- [112] Y. You, H.R. Yao, S. Xin, Y.X. Yin, T.T. Zuo, C.P. Yang, Y.G. Guo, Y. Cui, L.J. Wan, J.B. Goodenough, Subzero-temperature cathode for a sodium-ion battery, *Adv. Mater.* 28 (2016) 7243–7248, <https://doi.org/10.1002/adma.201600846>
- [113] Y.F. Yue, A.J. Binder, B.K. Guo, Z.Y. Zhang, Z.A. Qiao, C.C. Tian, S. Dai, Mesoporous prussian blue analogues: template-free synthesis and sodium-ion battery applications, *Angew. Chem. Int. Ed.* 53 (2014) 3134–3137, <https://doi.org/10.1002/anie.201310679>
- [114] X.H. Ma, Y.Y. Wei, Y.D. Wu, J. Wang, W. Jia, J.H. Zhou, Z.F. Zi, J.M. Dai, High crystalline Na<sub>2</sub>Ni[Fe(CN)<sub>6</sub>] particles for a high-stability and low temperature sodium-ion batteries cathode, *Electrochim. Acta* 297 (2019) 392–397, <https://doi.org/10.1016/j.electacta.2018.11.063>
- [115] J.Z. Sheng, H. Zang, C.J. Tang, Q.Y. An, Q.L. Wei, G.B. Zhang, L.N. Chen, C. Peng, L.Q. Mai, Graphene wrapped NASICON-type Fe<sub>2</sub>(MoO<sub>4</sub>)<sub>3</sub> nanoparticles as a ultrahigh rate cathode for sodium ion batteries, *Nano Energy* 24 (2016) 130–138, <https://doi.org/10.1016/j.nanoen.2016.04.021>
- [116] Y.N. Xu, Q.L. Wei, C. Xu, Q.D. Li, Q.Y. An, P.F. Zhang, J.Z. Sheng, L. Zhou, L.Q. Mai, Layer-by-layer Na<sub>3</sub>V<sub>2</sub>(PO<sub>4</sub>)<sub>3</sub> embedded in reduced graphene oxide as superior rate and ultralong-life sodium-ion battery cathode, *Adv. Energy Mater.* 6 (2016), <https://doi.org/10.1002/aenm.201600389>
- [117] G. Deng, D.L. Chao, Y.W. Guo, Z. Chen, H.H. Wang, S.V. Savilov, J.Y. Lin, Z.X. Shen, Graphene quantum dots-shielded Na<sub>3</sub>(VO)<sub>2</sub>(PO<sub>4</sub>)<sub>2</sub>F@C nanocuboids as robust cathode for Na-ion battery, *Energy Storage Mater.* 5 (2016) 198–204, <https://doi.org/10.1016/j.ensm.2016.07.007>
- [118] J.Z. Guo, P.F. Wang, X.L. Wu, X.H. Zhang, Q.Y. Yan, H. Chen, J.P. Zhang, Y.G. Guo, High-energy/power and low temperature cathode for sodium-ion batteries: in situ XRD study and superior full-cell performance, *Adv. Mater.* 29 (2017), <https://doi.org/10.1002/adma.201701968>
- [119] J.Z. Guo, Y. Yang, D.S. Liu, X.L. Wu, B.H. Hou, W.L. Pang, K.C. Huang, J.P. Zhang, Z.M. SU, A practicable Li/Na-ion hybrid full battery assembled by a high-voltage cathode and commercial graphite anode: superior energy storage performance and working mechanism, *Adv. Energy Mater.* 8 (2018), <https://doi.org/10.1002/aenm.201702504>
- [120] Y.Y. Wang, B.H. Hou, J.Z. Guo, Q.L. Ning, W.L. Pang, J.W. Wang, C.L. Lu, X.L. Wu, An ultralong lifespan and low-temperature workable sodium-ion full battery for stationary energy storage, *Adv. Energy Mater.* 8 (2018), <https://doi.org/10.1002/aenm.201703252>
- [121] X.L. Dong, Y. Yang, B.L. Wang, Y.J. Cao, N. Wang, P.L. Li, Y.G. Wang, Y.Y. Xia, Low-temperature charge/discharge of rechargeable battery realized by intercalation pseudocapacitive behavior, *Adv. Sci.* 7 (2020), <https://doi.org/10.1002/advs.202000196>
- [122] X.H. Rui, X.H. Zhang, S.T. Xu, H.T. Tan, Y. Jiang, L.Y. Gan, Y.Z. Feng, C.C. Li, Y. Yu, A low-temperature sodium-ion full battery: superb kinetics and cycling stability, *Adv. Funct. Mater.* 31 (2021), <https://doi.org/10.1002/adfm.202009458>
- [123] Z.Q. Lv, M.X. Ling, H.M. Yi, H.M. Zhang, Q. Zheng, X.F. Li, Electrode design for high-performance sodium-ion batteries: coupling nanorod-assembled Na<sub>3</sub>V<sub>2</sub>(PO<sub>4</sub>)<sub>3</sub>@C microspheres with a 3D conductive charge transport network, *ACS Appl. Mater. Interfaces* 12 (2020) 13869–13877, <https://doi.org/10.1021/acsami.9b22746>
- [124] B.L. Xu, S.H. Qin, M.M. Jin, X.Y. Cai, L.F. Lai, Z.T. Sun, X.G. Han, Z.F. Lin, H. Shao, P. Peng, Z.H. Xiang, J.E.T. Elshof, R. tan, C. Liu, Z.X. Zhang, X.C. Duan, J.M. Ma, 2020 roadmap on two-dimensional materials for energy storage and conversion, *Chin. Chem. Lett.* 30 (2019) 2053–2064, <https://doi.org/10.1016/j.ccl.2019.10.028>
- [125] J.M. Lim, T. Hwang, D. Kim, M.S. Park, K. Cho, M. Cho, Intrinsic origins of crack generation in Ni-rich LiNi<sub>0.8</sub>Co<sub>0.1</sub>Mn<sub>0.1</sub>O<sub>2</sub> layered oxide cathode material, *Sci. Rep.* 7 (2017) 1–10, <https://doi.org/10.1038/srep39669>
- [126] L. Mu, X. Feng, R. Kou, Y. Zhang, H. Guo, C. Tian, C.J. Sun, X.W. Du, D. Nordlund, H.L. Xin, F. Lin, Deciphering the cathode-electrolyte interfacial chemistry in sodium layered cathode materials, *Adv. Energy Mater.* 8 (2018), <https://doi.org/10.1002/aenm.201801975>
- [127] K. Wang, P. Yan, M. Sui, Phase transition induced cracking plaguing layered cathode for sodium-ion battery, *Nano Energy* 54 (2018) 148–155, <https://doi.org/10.1016/j.nanoen.2018.09.073>
- [128] K. Kaliyappan, J. Liu, B. Xiao, A. Lushington, R. Li, T.K. Sham, X. Sun, Enhanced performance of P2-Na<sub>0.66</sub>(Mn<sub>0.54</sub>Co<sub>0.13</sub>Ni<sub>0.13</sub>)O<sub>2</sub> cathode for sodium-ion batteries by ultrathin metal oxide coatings via atomic layer deposition, *Adv. Funct. Mater.* 27 (2017), <https://doi.org/10.1002/adfm.201701870>
- [129] Y. Li, Q.H. Shi, X.P. Yin, J. Wang, J. Wang, Y.F. Zhao, J.J. Zhang, Construction naxicon-type NaTi<sub>2</sub>(PO<sub>4</sub>)<sub>3</sub> nanoshell on the surface of P2-type Na<sub>0.67</sub>Co<sub>0.2</sub>Mn<sub>0.8</sub>O<sub>2</sub> cathode for superior room/low temperature sodium storage, *Chem. Eng. J.* 402 (2020), <https://doi.org/10.1016/j.cej.2020.126181>
- [130] Y. Li, Y.F. Zhao, X.C. Feng, X. Wang, Q.H. Shi, J. Wang, J.J. Zhang, Y.L. Hou, A durable P2-type layered oxide cathode with superior low temperature performance for sodium-ion batteries, *Sci. China Mater.* 65 (2022) 328–336, <https://doi.org/10.1007/s40843-021-1742-8>
- [131] M. Rashad, X.F. Li, H.M. Zhang, Magnesium/lithium-ion hybrid battery with high reversibility by employing NaV<sub>3</sub>O<sub>8</sub>·1.69H<sub>2</sub>O nanobelts as a positive electrode, *ACS Appl. Mater. Interfaces* 10 (2018) 21313–21320, <https://doi.org/10.1021/acsami.8b04139>
- [132] X.F. Bian, Y. Gao, S. Indris, Y.M. Ju, Y. Meng, F. Du, N. Bramnik, H. Ehrenberg, Y.L. Wei, A long cycle-life and high safety Na<sup>+</sup>/Mg<sup>2+</sup> hybrid-ion battery built by

- using a TiS<sub>2</sub> derived titanium sulfide cathode, *J. Mater. Chem. A* 5 (2017) 600–608, <https://doi.org/10.1039/C6TA08505A>
- [133] Z.H. Zhang, H.M. Xu, Z.L. Cui, P. Hu, J.C. Chai, H.P. Du, J.J. He, J.J. Zhang, X.H. Zhou, P.X. Han, G.L. Cui, L.Q. Chen, High energy density hybrid Mg<sup>2+</sup>/Li<sup>+</sup> battery with superior ultrahigh temperature performance, *J. Mater. Chem. A* 4 (2016) 2277–2285, <https://doi.org/10.1039/C5TA09591C>
- [134] M. Hu, X.L. Pang, Z. Zhou, Recent progress in high-voltage lithium ion batteries, *J. Power Sources* 237 (2013) 229–242, <https://doi.org/10.1016/j.jpowsour.2013.03.024>
- [135] W. Xu, J.L. Wang, F. Ding, X.L. Chen, E. Nasybulin, Y.H. Zhang, J.G. Zhang, Lithium metal anodes for rechargeable batteries, *Energy Environ. Sci.* 7 (2014) 513–537, <https://doi.org/10.1039/C3EE40795K>
- [136] L.A. Selis, J.M. Seminario, Dendrite formation in silicon anodes of lithium-ion batteries, *RSC Adv.* 8 (2018) 5255–5267, <https://doi.org/10.1039/C7RA12690E>
- [137] M. Rashad, H.Z. Zhang, X.F. Li, H.M. Zhang, Fast kinetics of Mg<sup>2+</sup>/Li<sup>+</sup> hybrid ions in a polyanion Li<sub>3</sub>V<sub>2</sub>(PO<sub>4</sub>)<sub>3</sub> cathode in a wide temperature range, *J. Mater. Chem. A* 7 (2019) 9968–9976, <https://doi.org/10.1039/C9TA00502A>
- [138] Q.Y. An, F. Lv, Q.Q. Liu, C.H. Han, K.N. Zhao, J.Z. Sheng, Q.L. Wei, M.Y. Yan, L.Q. Mai, Amorphous vanadium oxide matrices supporting hierarchical porous Fe<sub>3</sub>O<sub>4</sub>/graphene nanowires as a high-rate lithium storage anode, *Nano Lett.* 14 (2014) 6250–6256, <https://doi.org/10.1021/nl5025694>
- [139] D. Wang, Q.L. Wei, J.Z. Sheng, P. Hu, M.Y. Yan, R.M. Sun, X.M. Xu, Q.Y. An, L.Q. Mai, Flexible additive free H<sub>2</sub>V<sub>3</sub>O<sub>8</sub> nanowire membrane as cathode for sodium ion batteries, *Phys. Chem. Chem. Phys.* 18 (2016) 12074–12079, <https://doi.org/10.1039/C6CP00745G>
- [140] Y. Mettan, R. Caputo, T. Chatterji, A theoretical and experimental study of the crystal structure of H<sub>2</sub>V<sub>3</sub>O<sub>8</sub>, *RSC Adv.* 5 (2015) 106543–106550, <https://doi.org/10.1039/C5RA19665E>
- [141] H. Tang, N. Xu, C.Y. Pei, F.Y. Xiong, S.S. Tan, W. Luo, Q.Y. An, L.Q. Mai, H<sub>2</sub>V<sub>3</sub>O<sub>8</sub> nanowires as high-capacity cathode materials for magnesium-based battery, *ACS Appl. Mater. Interfaces* 9 (2017) 28667–28673, <https://doi.org/10.1021/acsami.7b09924>
- [142] J.H. Choi, W.H. Ryu, K. Park, J.D. Jo, S.M. Jo, D.S. Lim, I.D. Kim, Multilayer electrode with nano-Li<sub>4</sub>Ti<sub>5</sub>O<sub>12</sub> aggregates sandwiched between carbon nanotube and graphene networks for high power Li-ion batteries, *Sci. Rep.* 4 (2014) 1–7, <https://doi.org/10.1038/srep07334>
- [143] M. Rashad, M. Asif, Understanding the low temperature electrochemistry of magnesium-lithium hybrid ion battery in all-phenyl-complex solutions, *J. Energy Chem.* 56 (2021) 383–390, <https://doi.org/10.1016/j.jechem.2020.08.018>
- [144] C.J. Xu, B.H. Li, H.D. Du, F.Y. Kang, Energetic zinc ion chemistry: the rechargeable zinc ion battery, *Angew. Chem.* 124 (2012) 957–959, <https://doi.org/10.1002/anie.201106307>
- [145] H.F. Li, C.J. Xu, C.P. Han, Y.Y. Chen, C.G. Wei, B.H. Li, F.Y. Kang, Enhancement on cycle performance of Zn anodes by activated carbon modification for neutral rechargeable zinc ion batteries, *J. Electrochem. Soc.* 162 (2015), <https://doi.org/10.1149/2.0141508jes>
- [146] B. Lee, H.R. Lee, H. Kim, K.Y. Chung, B.W. Cho, S.H. Oh, Elucidating the intercalation mechanism of zinc ions into α-MnO<sub>2</sub> for rechargeable zinc batteries, *Chem. Commun.* 51 (2015) 9265–9268, <https://doi.org/10.1039/C5CC02585K>
- [147] P. Canepa, G.S. Gautam, D.C. Hanah, R. Malik, M. Liu, K.G. Gallagher, K.A. Persson, G. Ceder, Odyssey of multivalent cathode materials: open questions and future challenges, *Chem. Rev.* 117 (2017) 4287–4341, <https://doi.org/10.1021/acs.chemrev.6b00614>
- [148] P. He, G.B. Zhang, X.B. Liao, M.Y. Yan, X. Xu, Q.Y. An, J. Liu, L.Q. Mai, Sodium ion stabilized vanadium oxide nanowire cathode for high-performance zinc-ion batteries, *Adv. Energy Mater.* 8 (2018), <https://doi.org/10.1002/aenm.201702463>
- [149] H.G. Qin, Z.H. Yang, L.L. Chen, X. Chen, L.M. Wang, A high-rate aqueous rechargeable zinc ion battery based on the VS<sub>4</sub>@ rGO nanocomposite, *J. Mater. Chem. A* 6 (2018) 23757–23765, <https://doi.org/10.1039/C8TA08133F>
- [150] B.Y. Tang, J. Zhou, G.Z. Fang, S. Guo, X. Guo, L.T. Shan, Y. Tang, S.Q. Liang, Structural modification of V<sub>2</sub>O<sub>5</sub> as high-performance aqueous zinc-ion battery cathode, *J. Electrochem. Soc.* 166 (2019), <https://doi.org/10.1149/2.0081904jes>
- [151] J. Zhou, L.T. Shan, Z.X. Wu, X. Guo, G.Z. Fang, S.Q. Liang, Investigation of V<sub>2</sub>O<sub>5</sub> as a low-cost rechargeable aqueous zinc ion battery cathode, *Chem. Commun.* 54 (2018) 4457–4460, <https://doi.org/10.1039/C8CC02250J>
- [152] Y.Q. Yang, Y. Tang, G.Z. Fang, L.T. Shan, J.S. Guo, W.Y. Zhang, C. Wang, L.B. Wang, J. Zhou, S.Q. Liang, Li<sup>+</sup> intercalated V<sub>2</sub>O<sub>5</sub>·nH<sub>2</sub>O with enlarged layer spacing and fast ion diffusion as an aqueous zinc-ion battery cathode, *Energy Environ. Sci.* 11 (2018) 3157–3162, <https://doi.org/10.1039/C8EE01651H>
- [153] L.Y. Zhang, L. Chen, X.F. Zhou, Z.P. Liu, Towards high-voltage aqueous metal-ion batteries beyond 1.5 V: the zinc/zinc hexacyanoferrate system, *Adv. Energy Mater.* 5 (2015), <https://doi.org/10.1002/aenm.201400930>
- [154] P. He, Y.L. Quan, X. Xu, M.Y. Yan, W. Yang, Q.Y. An, L. He, L.Q. Mai, High-performance aqueous zinc-ion battery based on layered H<sub>2</sub>V<sub>3</sub>O<sub>8</sub> nanowire cathode, *Small* 14 (2017), <https://doi.org/10.1002/sml.201702551>
- [155] H.B. Geng, M. Cheng, B. Wang, Y. Yang, Y.F. Zhang, C.C. Li, Electronic structure regulation of layered vanadium oxide via interlayer doping strategy toward superior high-rate and low-temperature zinc-ion batteries, *Adv. Funct. Mater.* 30 (2020), <https://doi.org/10.1002/adfm.201907684>
- [156] Y. Luo, L.C. Wei, H.B. Geng, Y.F. Zhang, Y. Yang, C.C. Li, Amorphous Fe–V–O bimetallic oxides with tunable compositions towards rechargeable Zn-ion batteries with excellent low temperature performance, *ACS Appl. Mater. Interfaces* 12 (2020) 11753–11760, <https://doi.org/10.1021/acsami.0c00057>
- [157] Q. Zhang, K. Xia, Y.L. Ma, Y. Lu, L. Li, J. Liang, S.L. Chou, J. Chen, Chaotropic anion and fast-kinetics cathode enabling low temperature aqueous Zn batteries, *ACS Energy Lett.* 6 (2021) 2704–2712, <https://doi.org/10.1021/acscenergylett.1c01054>
- [158] J.L. Wang, S.T. Zhuang, Y. Liu, Metal hexacyanoferrates-based adsorbents for cesium removal, *Coord. Chem. Rev.* (2018) 430–438, <https://doi.org/10.1016/j.ccr.2018.07.014>
- [159] L.B. Ren, J.G. Wang, H.Y. Liu, M.H. Shao, B.Q. Wei, Metal-organic-framework-derived hollow polyhedrons of prussian blue analogues for high power grid-scale energy storage, *Electrochim. Acta* 321 (2019), <https://doi.org/10.1016/j.electacta.2019.134671>
- [160] Z.X. Song, W. Liu, Q. Zhou, L. Zhang, Z. Zhang, H.D. Liu, J.Q. Du, J.L. Chen, G.C. Liu, Z.F. Zhao, Cobalt hexacyanoferrate/MnO<sub>2</sub> nanocomposite for asymmetrical supercapacitors with enhanced electrochemical performance and its charge storage mechanism, *J. Power Sources* 465 (2020), <https://doi.org/10.1016/j.jpowsour.2020.228266>
- [161] J. Gu, K. Cui, S. Niu, Y. Ge, Y.H. Liu, Z.Y. Ma, C. Wang, X.Y. Li, X.Y. Wang, Smart configuration of cobalt hexacyanoferrate assembled on carbon fiber cloths for fast aqueous flexible sodium ion pseudocapacitor, *J. Colloid Interface Sci.* 594 (2021) 522–530, <https://doi.org/10.1016/j.jcis.2021.03.031>
- [162] X.J. Zhang, L. Tao, P. He, X.Q. Zhang, M.Q. He, F.Q. Dong, S.Y. He, C.X. Li, H.H. Liu, S. Wang, Y. Zhang, A novel cobalt hexacyanoferrate/multi-walled carbon nanotubes nanocomposite: spontaneous assembly synthesis and application as electrode materials with significantly improved capacitance for supercapacitors, *Electrochim. Acta* 259 (2018) 793–802, <https://doi.org/10.1016/j.electacta.2017.11.007>
- [163] Z.X. Song, W. Liu, Q. Yuan, Q. Zhou, G.C. Liu, Z.F. Zhao, Microporous/mesoporous cobalt hexacyanoferrate nanocubes for long-cycle life asymmetric supercapacitors, *J. Mater. Sci. Mater. Electron.* 29 (2018) 14897–14905, <https://doi.org/10.1007/s10854-018-9628-5>
- [164] F.P. Zhao, Y.Y. Wang, X.N. Xu, Y.L. Liu, R. Song, G. Lu, Y.G. Li, Cobalt hexacyanoferrate nanoparticles as a high-rate and ultra-stable supercapacitor electrode material, *ACS Appl. Mater. Interfaces* 6 (2014) 11007–11012, <https://doi.org/10.1021/am503375h>
- [165] J. Chen, K.L. Huang, S.Q. Liu, Insoluble metal hexacyanoferrates as supercapacitor electrodes, *Electrochem. Commun.* 10 (2008) 1851–1855, <https://doi.org/10.1016/j.elecom.2008.07.046>
- [166] L.T. Mao, S.M. Chen, N. Li, Z.X. Liu, Z.J. Tang, J.A. Zapien, S.M. Chen, J. Fan, C.Y. Zhi, Hydrogen-free and dendrite-free all-solid-state Zn-ion batteries, *Adv. Mater.* 32 (2020), <https://doi.org/10.1002/adma.201908121>
- [167] N.A. Kumar, H.J. Choi, Y.R. Shin, D.W. Chang, L.M. Dai, J.B. Baek, Polyaniline-grafted reduced graphene oxide for efficient electrochemical supercapacitors, *ACS Nano* 6 (2012) 1715–1723, <https://doi.org/10.1021/nn204688c>
- [168] H. Sun, S.L. Xie, Y.M. Li, Y.S. Jiang, X.M. Sun, B.J. Wang, H.S. Peng, Large-area supercapacitor textiles with novel hierarchical conducting structures, *Adv. Mater.* 38 (2016) 8431–8438, <https://doi.org/10.1002/adma.201602987>
- [169] Y. Xia, D.R. Zhu, S.H. Si, D.G. Li, S. Wu, Nickel foam-supported polyaniline cathode prepared with electrophoresis for improvement of rechargeable Zn battery performance, *J. Power Sources* 283 (2015) 125–131, <https://doi.org/10.1016/j.jpowsour.2015.02.123>
- [170] K. Ghanbari, M.F. Mousavi, M. Shamsipur, H. Karami, Synthesis of polyaniline/graphite composite as a cathode of Zn-polyaniline rechargeable battery, *J. Power Sources* 170 (2007) 513–519, <https://doi.org/10.1016/j.jpowsour.2007.02.090>
- [171] P. Jimenez, E. Levillain, O. Aleveque, D. Guyomard, B. Lestriez, J. Gaybicher, Lithium n-doped polyaniline as a high-performance electroactive material for rechargeable batteries, *Angew. Chem. Int. Ed.* 56 (2017) 1553–1556, <https://doi.org/10.1002/anie.201607820>
- [172] X.D. Lin, G.D. Zhou, M.J. Robson, J. Yu, S.C.T. Kwok, F. Ciucci, Hydrated deep eutectic electrolytes for high-performance Zn-ion batteries capable of low-temperature operation, *Adv. Funct. Mater.* 32 (2021), <https://doi.org/10.1002/adfm.202109322>